ASTRONOMY & ASTROPHYSICS
SUPPLEMENT SERIES

DECEMBER I **1996**, PAGE 323

Astron. Astrophys. Suppl. Ser. **120,** 323-356 (1996)

Observations of a complete sample of Hα emission-line galaxies. Long-slit spectroscopy of galaxies in UCM lists 1 and 2*,**

J. Gallego***, J. Zamorano, M. Rego, O. Alonso and A.G. Vitores†

Dpto Astrofísica, Universidad Complutense de Madrid, E-28040 Madrid, Spain

Received June 28, 1995; accepted May 2, 1996

Abstract. — Spectroscopic observations for the full sample of Hα emission–line galaxy candidates (ELGs) from the Universidad Complutense de Madrid objective-prism survey Lists 1 and 2 have been obtained in order to investigate fully the properties of the survey constituents as well as the selection characteristics and completeness limits of the survey itself. The spectroscopic data include redshifts, line fluxes, equivalent widths, emission-line ratios, optical reddening estimates and synthesized color indexes. We find that 74% of the objects in this sample do exhibit emission lines. We compare our observational data with parameters given in the published survey lists in order to assess the usefulness of the latter. The different emission-line galaxies have been classified according to their spectra in several groups. Gray-scale images of the CCD spectra near the main emission lines, spatial profiles at the continuum and the line for [OIII] λ5007 and Hα lines, as well as plots of the coadded spectra of selected galaxies are presented, and a number of peculiar objects are described.

Key words: galaxies: redshifts; starburst — surveys

1. Introduction

The UCM Hα objective-prism survey is being carried out with the main purposes of identifying and studying new young, low metallicity galaxies and quantifying the properties of the star formation in the local universe. To achieve these final goals we need to characterize both spectroscopic and photometrically the emission-line galaxies (ELGs) found by their Hα+[NII] emission at the Schmidt plates of the UCM sample. Because the specific details of the UCM survey have already been summarized in the first list (Zamorano et al. 1994) and completed in the second list (Zamorano et al. 1996) of our exploration, and the photometric aspects of the sample are presented in Vitores et al. (1996), we only concentrate here in the spectroscopic characteristics of the survey.

Although there are already several studies (Wasilewski 1983; Salzer et al. 1989; Rosenberg & Salzer 1994) about the samples of ELGs obtained using the objective-prism technique for emission lines at the blue part of the optical spectrum, to date no systematic and complete follow-up investigations have been carried out on a objective-prism sample obtained in the Hα line. In particular no complete accounting of the survey contents or a proper determination of the completeness limits of this kind of survey has appeared in print.

Given the obvious importance of the comparison between the results of a survey in the blue and another similar in the red in order to determine the differences in the population obtained with both techniques (Markarian et al. 1987; Boroson et al. 1993; Zamorano et al. 1994; Zamorano et al. 1996; Gallego 1995) we have carried out a program of obtaining CCD spectroscopy of the whole sample of ELGs candidates discovered in the UCM survey. The goals of this study are (1) to determine the selection characteristics, biases, and completeness limits of the UCM survey, (2) to study the relationships between the line-emitting regions and the host galaxies within which

Send offprint requests to: J. Gallego

*Partly based on observations collected at the German-Spanish Astronomical Center, Calar Alto, Spain, operated by the Max-Planck-Institut für Astronomie (MPIA), Heidelberg, jointly with the Spanish National Commission for Astronomy. Partly based on observations made with the Isaac Newton Telescope operated on the island of La Palma by the Royal Greenwich Observatory in the Spanish Observatorio del Roque de Los Muchachos of the Instituto de Astrofísica de Canarias

**Table 4 is only available in electronic form at CDS via anonymous ftp 130.79.128.5 or on www at http://cdsweb.u-strasbg.fr/abstract.html. Table 5 is also available in electronic form at CDS

****Present address*: UCO/Lick Observatory, University of California, Santa Cruz, CA95064

†EUIT Industrial. Universidad Politécnica, E-28012, Madrid, Spain they reside, and (3) to study the spatial and luminosity distributions of the UCM ELGs to determine how they compare with those of other ELGs surveys and normal galaxies.

The current paper presents our observational data, while a discussion of the properties of the UCM galaxies and a detailed analysis of the spatial and luminosity distributions are given in an incoming paper. A companion study of the far-infrared properties of this sample of ELGs may be found in Rego et al. (1993).

2. Observations

2.1. *Data acquisition*

Table 1 lists the ten observing runs during which the spectroscopic observations were carried out. The telescopes used were the 3.5 m and the 2.2 m of the CAHA Observatory (Calar Alto German-Spanish Observatory at Almería, Spain) and the 2.5 m Isaac Newton Telescope (INT) of the Roque de los Muchachos Observatory (La Palma, Spain). The Col. (3) gives the spectrograph utilized, always at the Cassegrain focus, except the 1990 run at the 3.5 m telescope during which we experimented the grism (grating + prism) available at the prime focus. IDS is for the Intermediate Dispersion Spectrograph of the 2.5 m at Roque de los Muchachos. The Col.(4) gives the detector used, always a CCD chip except for the IPCS (Image Photon Counting System, Boksenberg 1972; Jenkins 1986). The wavelength range covered, the dispersion and the spatial scale are given in Cols. (5)-(7). Finally the Col. (8) gives the slit width in arc-sec adopted for each run. After the June 1991 run CCD images taken for most of all objects with the 2.2 m Calar Alto telescope (Vitores et al. 1996) were accessible. Using these frames the slit was, when possible, oriented along the mayor axis of the galaxy.

In addition to the program objects, various calibration observations were obtained during each run. Wavelength comparison lamps were observed before and after each time the telescope position was shifted more than a few degrees. Flat field frames were acquired each night using tungsten lamps for fixing low and high frequency variations over the chip. In addition several spectrophotometric standard stars were observed each night in order to establish the spectral sensitivity function for flux calibration. These standards are from the lists of Oke (1974), Strom (1977) and Oke & Gunn (1983).

Total integration times varied from the first run to the last one. The exposure time depended primarily on the instrumental setup, the efficiency of the detector and the brightness of the target. For the 1986 runs one hour was the standard. During the last runs at the INT five minutes were enough to achieve a good signal-to-noise ratio. The whole sample of UCM ELG candidates were observed spectroscopically, including near spirals previously known. The high degree of completeness wanted when scanning the Schmidt plates provided a high fraction of candidates not confirmed as emission-line galaxies. A summary indicating the classification type of all objects included in this study, both ELGs and non-ELGs, is given in Sect. 5.

2.2. *Data reduction*

The reduction of the data was performed in several stages. The first one, in order to eliminate the detector effects in the two-dimension frames, was done following the standard procedure of cosmic-rays and bias removal, dark-current subtraction and flat fielding using the ESO MIDAS image processing system. The second one was carried out after extracting the unidimensional spectrum for each of every emission knot present at each galaxy. When the knot had a measurable size a simple integration in the spatial direction was done. In the case of punctual sources the optimization algorithm implemented in MIDAS (Horne 1986) was applied. In the course of this step the sky was subtracted from each frame by interactively selecting regions on either side of the object's spectrum which contained flux from the sky only. At each scan along the dispersion direction, the sky pixels were fitted by a polynomial of low order, and the sky values under the object spectrum were evaluated interpolating the polynomial between the two sky regions.

Scans of copper, argon, helium and neon lamps were used to determine an accurate wavelength scale ($\sigma \sim$ 0.2 Å), and the results were used to re-bin the data onto a linear wavelength scale. Standard star observations yielded sensitivity curves which converted the observed count rates per pixel to flux density units. After the galaxy and the standard star spectra were corrected for atmospheric extinction using mean La Palma extinction coefficients (King 1985), the sensitivity curve was applied to each galaxy spectrum.

The IPCS spectra were reduced considering an extra stage. Before of extracting the unidimensional spectrum it was necessary to check for any geometrical defect induced by the electronic nature of this detector. This work was done using the emission lines present at the sky and the lines of the arc frames. The corrections were always small and only necessary at the edge of the original frames.

2.3. *Astronomical data*

Once fully reduced, the emission lines in each spectrum were measured for line centers, fluxes and equivalent widths. The fundamental observed quantities obtained from the spectroscopic data for all the objects with emission confirmed are summarized in Tables 4 and 5. Line fluxes relatives to Hβ=100 for all the emission lines detected are summarized in Table 4 for each galaxy. In case of no Hβ line apparent, the fluxes are given relatives to Hα=100. Column (1) gives the UCM name. The first line of the rest of columns gives the observed values whereas

Table 1. Spectroscopic observing runs

Dates run	Telescope	Instrument	Detector	range λλ Å	Δ_λ Å/pix	scale ″/pix	slit width
1986 Dec 1-8	CAHA 2.2 m	Boller & Chivens	RCA#11	4200-7600	7.20	1″40	2″5
1988 Dec 22-23	2.5 m INT	IDS 235 mm	IPCS	3700-7600	2.08	1″66	2″0
1989 Nov 3-6	CAHA 3.5 m	Double sp	RCA	4000-5000	2.40	0″65	2″4
			GEC	6000-7200	1.84	1″00	2″4
1990 Jun 18-20	CAHA 3.5 m	Focal Reducer	RCA#11	4200-7200	4.10	0″50	2″6
1991 Jun 11-16	2.5 m INT	IDS 235 mm	IPCS	3700-7600	2.08	1″66	2″2
1993 Jan 20-24	CAHA 2.2 m	Boller & Chivens	Tek#6	4330-7050	2.90	1″40	2″5
1993 Aug 13-15	CAHA 2.2 m	Boller & Chivens	Tek#6	4330-7050	2.90	1″40	2″5
1993 Nov 11-14	2.5 m INT	IDS 235 mm	EEV5	3720-7100	3.05	0″60	4″0
1994 Jul 2-6	2.5 m INT	IDS 235 mm	Tek#3	3700-7100	3.30	0″71	4″0
1994 Sep 10-14	2.5 m INT	IDS 235 mm	Tek#3	3700-7100	3.30	0″71	2″0

the reddening-corrected ones are presented in the second line. The Table 5 lists in Col. (1) the UCM name, in Col. (2) the heliocentric redshift, z, in Col. (3) the signal-to-noise ratio at the continuum near Hα as estimated by computing the ratio between the σ in a 100 Å band centered at 6450 Å (rest wavelength) and the mean flux in the same range, and in Cols. (4)-(7) the equivalent widths in angstroms for [OII]λ3727, Hβ, [OIII]λ5007 and Hα emission lines. The Cols. (8) and (9) of the same table give the observed Hβ and Hα line fluxes, Cols. (10) and (11) the synthetic $b-v$ and $v-r$ color indexes, Col. (12) the $B-V$ color excess and Col. (13) the observed Hα luminosity in solar units. The quoted redshift is the mean of those determined from individual strong lines, weighted with the equivalent widths. Despite the Hα line is blended, it was used for redshift determination because for most of the UCM galaxies it is the brightest line. Typical uncertainties in z range from ~ 30 km s^{-1} to ~ 100 km s^{-1} for galaxies with weak lines. The equivalent widths were measured interactively fitting the continuum with a low-order polynomial. The Balmer lines fluxes are given in units of 10^{-14} erg cm^{-2} s^{-1}. The synthetic color indexes were computed from the monochromatic magnitudes obtained with 100 Å bands. The color excess was computed using either the Hγ/Hβ or Hα/Hβ intensity ratios. The intrinsic ratios of $I(\mathrm{H}\alpha)/I(\mathrm{H}\beta)$=2.86 and $I(\mathrm{H}\gamma)/I(\mathrm{H}\beta)$=0.468 corresponding to the theoretical values for a low density gas with T_e=10000 K were adopted (Osterbrock 1989). The measurement of the observed line ratios can be fairly imprecise, which will result in substantial uncertainties in the reddening coefficient. A colon following the value of E_{B-V} indicates a particularly uncertain value because Hβ was weak (WHβ <20 Å). For some galaxies, it was not possible to compute the color excess. In these cases the column is blank.

3. Comments on specific objects

In this section we will describe several objects which appear to be particularly unusual, even for this sample of strong Hα emission galaxies. Gray-scale and plots of the spectra are presented for selected UCM ELGs in Appendix A. A more detailed description for the entire UCM sample can be found in Gallego (1995). All distance-dependent parameters discussed below are derived using H_0 = 50 km s^{-1} Mpc^{-1}.

3.1. *Seyfert galaxies*

A total of 14 Seyfert galaxies (5%) were found in UCM Lists 1 and 2. This proportion is smaller than other surveys for emission lines in the blue (11% for Universidad de Michigan –Salzer et al. 1989– and Markarian surveys –Mazzarella & Balzano 1986–) and is consequence of better efficiency of the UCM survey technique to detect low ionization and high extinction emission-line galaxies. This deficiency of Seyfert galaxies is only in relative numbers because in absolute terms the UCM survey detects each of Seyfert galaxies present in the fields analyzed and previously known. The same effect has been observed in the Case Survey for blue or emission-line galaxies (Salzer et al. 1995). A few of these objects are particularly noteworthy. UCM 2257+2438 is a Seyfert 1 galaxy not previously known. This object is a narrow-line Seyfert 1 placed in the nucleus of a Sa nearly face-on galaxy with a significant contribution of starlight (Zamorano et al. 1992). UCM 2329+2500 is a rather interesting Seyfert 1 galaxy. The nuclear spectrum presents broad components (FWHM= 8000 km s^{-1}) and asymmetric profiles at the Balmer lines showing a secondary peak more apparent on the Hβ line and also observed in the Hα line. Eight kpc away from the nucleus a ring-like structure with emission that surrounds the core is observed (Gallego et al. 1994). A very similar spectrum is present at UCM 2333+2359, but better observational data are needed in this case. Of the nine Seyfert 2 only two were not previously known. UCM 0119+2156 is a high luminosity galaxy which most peculiar characteristic is that it does not show any Hβ emission. UCM 2303+1702 displays emission lines with a blue-ward asymmetry and appears as a Sc$^+$ spiral nearly face-on that hosts a Seyfert 2 nucleus (Rego et al. 1994). A total of three ELGs show spectral features typical of the LINER phenomena. UCM 0040−0023, UCM 0129+2109 and UCM 2317+2356, all showing a low ionization spectrum with strong [NII] λ6584 and [SII] $\lambda\lambda$6716, 6731 lines.

3.2. *Interacting galaxies*

A subset of galaxies appears very close in the sky, being candidates to systems with real interacting processes. UCM 1440+2521N and UCM 1440+2521S are two nuclear starburst galaxies with evidences of interaction. UCM 2255+1930N and UCM 2255+1930S seem to be another binary system with strong low ionization emission induced by the encounter. The same scenario is applicable to UCM 2327+2515, two galaxies situated south of a bright star. UCM 2325+2318 is a peculiar object with three components in emission. The main nucleus is connected with a small knot also in connection with a peripheral knot with EW(Hα)=400 Å.

3.3. *Galaxies with spectrum dominated by hot stars*

As can be expected from the selection technique used by the UCM survey, the main population are galaxies with strong emission lines. In this section we notice several ELGs with a compact shape, high equivalent widths and emission lines originated in species of high ionization. UCM 0049−0006 (previously known as UM282) is situated at 225 Mpc and shows very low extinction. All the Balmer lines are clearly seen at the spectrum. Finally, UCM 1304+2830, UCM 1324+2926, UCM 1331+2900, UCM 1429+2645 and UCM 1612+1308 are ELGs with a blue spectrum dominated by the emission of the nebular Hydrogen surrounding intense star formation regions.

Table 2. Comparison of the continuum parameter and the r apparent magnitude

Type UCM	$< m_r >$	σ	No
A	16.0	1.04	127
B	14.9	0.96	73
C	14.7	0.42	13

3.4. *Unusual objects*

Searching for all sources with Hα+[NII] in emission it is not surprising to find a number of objects that are specially remarkable. UCM 0056+0044 is a nearby low-luminosity galaxy with emission over all the object. It appears as an irregular galaxy undergoing a recent global star formation process. UCM 0148+2124 presents a double nucleus structure, both in emission but one of them much redder. UCM 1257+2754 has been confirmed as the planetary nebula PG 1257+279 (Acker et al. 1992). It is in the Coma cluster direction. UCM 2307+2119 corresponds to a symbiotic star with strong both Hβ and Hα lines in emission. It also shows weak HeI lines. UCM 2324+2448 is a nearby spiral galaxy with emission at the nucleus. This object shows a peculiar HII region at 47 arcsec North. It presents extremely high ionization properties. However not physical connection with the nucleus has been observed, both objects present the same redshift.

Table 3. UCM line contrast indicator as a function of the measured equivalent width

Tipo UCM	$< EW_{H\alpha+[NII]} >$	σ	No
A1	28	42	44
B1	35	34	37
	31	**38**	**81**
A2	100	78	49
B2	100	69	24
	100	**73**	**73**
A3	206	159	16
B3	148	45	9
	177	**102**	**25**
C1	134	134	6
C2	119	71	8

3.5. *Objects with no emission*

Due to the interest in recovering all the possible ELG candidates when the Schmidt plates were scanned, several candidates of the final lists resulted to be objects with no real emission. A total of seventy objects observed show no emission lines (43 galaxies and 27 stars). It was also found an emission-line star (UCM 2307+2119) and a planetary nebula (UCM 1257+2754). Therefore, the success rate of the UCM survey for detecting true emission-line objects is 74%. In Table 6a are listed the 39 candidates with no emission but without enough spectroscopic information for a final classification. In Table 6b are the 27 objects confirmed as field stars that were wrongly selected as ELG candidates. They are mainly red-giant stars with strong continua in the red. Finally in Table 6c are shown 10 previously known galaxies that did not present clear emission lines. When known, is given redshift, and from our data possible but not confirmed Hα+[NII] equivalent width in Å, and color indexes $b - v$ and $v - r$. Three of these galaxies (UCM 0053−0049, UCM 0138+2216 and

UCM 0139+2226) show traces of Hα in emission but any classification remains quite uncertain.

4. The UCM survey list parameters

The published discovery lists (Zamorano et al. 1994; Zamorano et al. 1996) of the UCM survey describe the appearance of the spectrum of each UCM ELG candidate on the objective-prism (OP) plates using two empirical parameters. Here we will compare the observational data obtained in this study with these list parameters in order to ascertain their reliability and to assess their usefulness.

Each UCM object was initially assigned a continuum parameter based on the brightness of the continuum near Hα. This magnitude refers only to the line-emitting region, and it has only three possibilities. A means a non-existent or very weak continuum. B means moderate continuum and C is for the almost saturated objects. The Table 2 compares the OP estimates against the total apparent r magnitude from Vitores et al. (1996) giving the mean value for each category, the standard deviation and the number of galaxies in the bin. It is clearly shown a general trend but the scatter is large, mainly due to the different sizes of the galaxies. A good example is UCM 2244+2049, a nearby spiral galaxy with a big apparent diameter. It has been classified with A because the emission is located at an extra-nuclear HII region. The opposite is UCM 1452+2754, an ultra compact object classified as C but with a faint r magnitude. It is clear that the OP parameter is a fairly useful estimate of the total magnitude of the galaxy.

Next we compare the OP contrast parameter (1 for low contrast line, 2 for medium contrast line and 3 for very high contrast) with the measurements of Hα+[NII] equivalent widths from the spectroscopic observations. The results are given in Table 3. The mean values have been detached for each contrast sub-category and continuum parameter. It is evident that the mean value increases from 1 to 2 and from 2 to 3. The objects classified with a continuum parameter C does not follow the general behavior. This is because for these objects the continuum is near to saturation and they do not show a normal proportional response. In consequence, when a C object has a high equivalent width it is not always reflected in the OP appearance. Sometimes the line is also saturated and the contrast results low. As can be seen in Table 3, the scatter is important. The standard deviations of the data are generally as large as the average values in each group. This large range in the measured quantities limits the predictive power of the contrast parameter.

5. Classification of the UCM emission-line galaxies

In this work we have adopted the classification proposed by Salzer et al. (1989) for classifying the ELGs discovered by the University of Michigan survey and also applied to the Case Survey (Rosenberg et al. 1994). The main physical properties considered for the classification are the emission line fluxes and equivalent widths, the Hα luminosity, the localization of the starburst process in the galaxy and its relative importance respect to the whole galaxy. We have not considered the *Magellanic irregulars, Giant irregular galaxies, and Interacting pairs* because they are not spectroscopically different. Each time we have found a pair of galaxies in interaction we have proceeded to classify individually each member of the system. The rest of categories have been maintained. A brief description of each ELG class follows.

Seyfert 1. The optical spectrum of these galaxies is dominated by a high ionization and it is characterized by emission lines from highly ionized species. The Hα luminosity is always greater than $10^8\ L_\odot$. The Balmer lines present broad components with FWHM ~ 1000 km s^{-1}. The most representative object in the UCM list is UCM 2329+2500.

Seyfert 2. They are characterized by certain emission lines specially strong. However, some line ratios are the actual indicators for the Seyfert 2 nature. The line [OIII] λ5007 is always much stronger than Hβ (typically [OIII] $\geq$ 3 Hβ), and [NII] λ6584 is comparable to Hα. Lines from high ionization species are also present.

LINER. These objects present a continuum with absorption lines and several low ionization emission lines. [OII] λ3727 is comparable or greater than [OIII] λ5007. The line [OI] λ6300 is specially strong and [NII] λ6584 is again comparable to Hα.

These first three ELG classes are usually denominated "active galaxies" due to a considerable amount of energy with non-thermal origin in the total output of the galaxy.

SBN. StarBurst Nuclei were originally defined by Balzano 1983. They are spiral galaxies that host a nucleus with an star-forming process. The extinction is important so in the blue part of the spectrum scarcely one can appreciate faint emission lines. The most prominent line is always Hα, being [NII] much weaker. Sometimes these galaxies present out of the nucleus HII regions with colors bluer than the central core. The Hα luminosity was always found greater than $10^8\ L_\odot$. As it will be analyzed in an incoming paper these galaxies are the most frequent in the UCM survey population.

DANS. The Dwarf Amorphous Nuclear Starburst are a new ELG class introduced by Salzer et al. (1989). This category contains galaxies similar to the SBN phenomena but at lower scale. They are spectroscopically indistinguishable from SBNs, but their Hα luminosities are always lower than $5\ 10^7\ L_\odot$. Good examples are UCM 0141+2220 and UCM 2256+2002.

HIIH. The HII Hotspot class has in this work a slightly different behavior. It includes all those galaxies with a global star-forming process and an optical spectrum dominated by blue colors and strong emission lines. Their

Table 5. Summary of spectroscopic data

UCM	z	SNR	EW(Å)				Flux*		$b-v$	$v-r$	E_{B-V}	$L_{\mathrm{H}\alpha}$	Spect
			[OII]	Hβ	[OIII]	Hα†	Hβ	Hα				$10^8\ L_\odot$	Type
0000+2140	0.0238	47	37	15	33	154	3.73	32.80	0.10	0.42	1.024	12.12	HIIH
0003+1955	0.0278	40	0	74	31	379	65.70	...	−0.41	0.17	...	103.20	Sy1
0003+2200	0.0224	15	0	5	9	50	0.25	1.82	0.22	0.28	0.867:	0.28	DANS
0003+2215	0.0223	18	0	4	0	36	0.23	2.01	0.48	0.71	1.008:	0.58	SBN
0005+1802	0.0187	20	0	1	2	19	0.06	0.68	0.63	0.59	1.244:	...	SBN
0006+2332	0.0159	22	46	9	21	67	0.83	4.82	0.04	0.19	0.644	2.13	HIIH
0013+1942	0.0272	6	98	30	72	142	1.08	4.18	−0.06	0.09	0.276	0.86	HIIH
0014+1748	0.0182	13	9	12	0	135	0.27	1.89	0.54	0.03	0.806	2.95	SBN
0014+1829	0.0182	13	27	6	22	146	0.13	1.81	−0.07	...	1.473	0.56	HIIH
0015+2212	0.0198	15	67	25	48	147	1.11	4.02	−0.12	−0.01	0.215	1.01	HIIH
0017+1942	0.0281	6	110	25	107	181	0.54	2.27	−0.30	−0.08	0.357	2.96	HIIH
b	0.0281	11	34	7	30	65	0.26	1.71	−0.01	0.04	0.778	1.06	HIIH
c	0.0281	6	75	17	66	107	0.28	1.15	...	−0.09	0.340	1.68	HIIH
0017+2148	0.0189	9	...	15	13	97	1.05	5.64	...	...	0.575	1.01	HIIH
0018+2215	0.0169	23	0	3	2	20	0.17	0.56	...	−0.20	0.136:	0.09	DANS
0018+2218	0.0220	20	0	0	0	14	0.00	0.72	0.67	0.84	...	0.09	SBN
0019+2201	0.0191	27	20	8	2	45	0.33	1.54	0.32	0.41	0.438	0.32	DANS
0022+2049	0.0185	10	45	11	5	106	0.90	6.93	0.62	0.10	0.901	1.83	HIIH
0023+1908	0.0251	17	...	24	25	157	0.80	3.59	0.02	0.09	0.409	...	HIIH
0034+2119	0.0315	17	40	3	7	24	0.19	1.15	0.32	0.46	0.684:	1.14	SBN
0037+2226	0.0204	18	22	7	3	57	0.33	1.85	0.15	0.22	0.615	2.75	SBN
a	0.0208	10	42	8	5	67	0.18	0.99	0.02	0.04	0.600	3.33	SBN
0038+2259	0.0464	9	0	4	0	27	0.13	0.88	0.35	0.32	0.810:	1.80	SBN
0039+0054	0.0191	13	0	0	0	22	0.00	0.82	0.17	0.31	...	0.38	SBN
0040−0023	0.0142	28	0	0	0	15	0.00	5.28	0.32	0.41	...	...	LINER
0040+0220	0.0173	15	48	18	18	97	0.73	3.16	0.04	0.26	0.378	0.25	DANS
0040+2312	0.0254	21	0	0	0	26	0.00	2.30	0.46	0.61	...	...	SBN
0040+0257	0.0367	17	45	0	11	196	0.00	5.11	0.41	−0.42	...	1.46	DANS
0041+0135	0.0169	15	0	0	0	13	0.00	0.93	−0.17	−0.07	...	...	DESC
0043−0159	0.0161	7	0	0	0	86	0.00	0.88	0.36	0.12	...	...	SBN
0043+0245	0.0180	18	69	4	19	38	0.15	1.24	0.28	0.13	0.950:	0.16	HIIH
0044+2246	0.0253	20	0	3	16	44	0.10	1.27	0.65	0.69	1.384	1.07	SBN
0045+2206	0.0203	21	43	13	16	99	2.16	10.60	−0.11	0.10	0.493	3.42	HIIH
0047−0213	0.0144	26	35	5	21	48	0.99	7.25	0.11	0.22	0.857	0.38	DHIIH
0047+2051	0.0577	9	21	12	4	109	0.43	2.39	0.13	0.55	0.598	4.38	SBN
0047+2413	0.0347	28	12	7	1	79	0.35	3.16	0.49	0.64	1.059	3.96	SBN
a	0.0343	13	55	20	11	133	0.34	1.68	0.16	0.35	0.497	6.17	SBN
c	0.0349	9	42	8	6	79	0.08	0.50	0.14	0.35	0.746	4.00	SBN
0047+2414	0.0347	28	24	14	7	112	0.94	5.15	0.06	0.35	0.592	8.52	SBN
0049−0045	0.0048	35	69	48	120	245	1.29	5.82	0.23	−0.03	0.416	...	HIIH
a	0.0049	30	35	5	13	37	0.58	3.31	0.05	−0.10	0.631	0.29	HIIH
0049−0006	0.0377	15	62	95	418	349	0.90	2.60	−0.36	0.20	0.006	0.77	BCD
0049+0017	0.0140	17	122	23	75	340	1.36	4.28	0.04	0.14	0.088	0.42	DHIIH
0050+0005	0.0346	18	51	19	57	115	0.13	0.60	−0.12	...	0.438	2.14	HIIH
0050+2114	0.0245	17	20	11	7	111	1.78	12.40	0.09	0.30	0.813	2.76	SBN
0051+2430	0.0173	18	0	5	24	67	0.33	2.94	0.62	0.59	1.040	1.45	SBN
0054−0133	0.0512	29	0	0	2	22	0.00	1.19	0.43	0.33	...	3.03	SBN
0054+2337	0.0164	11	36	9	7	71	0.24	1.45	0.09	0.10	0.667	1.38	HIIH
0056+0043	0.0189	15	33	21	27	61	1.00	4.11	−0.01	0.08	0.331	0.26	DHIIH
0056+0044	0.0183	6	105	82	294	420	0.69	2.14	−0.32	−0.04	0.079	0.76	DHIIH

* In units of 10^{-14} erg/cm²/s.

† Hα denote the blend Hα+[NII].

Table 5. continued

UCM	z	SNR	EW(Å)				Flux*		$b-v$	$v-r$	E_{B-V}	$L_{\mathrm{H}\alpha}$	Spect
			[OII]	Hβ	[OIII]	Hα†	Hβ	Hα				10^8 $L_\odot$	Type
0119+2156	0.0583	13	0	0	8	16	0.00	0.33	0.87	0.55	...	1.21	Sy2
0121+2137	0.0345	24	0	9	7	87	0.22	1.36	0.12	0.26	0.703	2.20	SBN
0129+2109	0.0344	8	0	0	0	32	0.00	1.59	−0.01	0.71	...	3.75	LINER
0134+2257	0.0353	31	0	4	7	43	0.15	1.17	0.53	0.59	0.892	0.69	SBN
0135+2242	0.0363	21	88	9	13	60	0.04	0.34	0.64	...	0.976	0.96	DANS
0138+2216	0.0591	16	9	1	2	15	0.03	0.31	0.84	0.43	1.086:	...	SBN
0141+2220	0.0174	20	26	6	3	48	0.53	3.41	0.17	0.33	0.742	0.25	DANS
0142+2137	0.0362	15	32	6	101	61	0.41	2.12	0.61	0.70	0.537	5.37	Sy2
0144+2519	0.0414	9	0	4	0	38	0.11	0.97	0.30	0.58	1.033:	2.60	SBN
0147+2309	0.0194	6	68	20	46	132	0.96	4.70	−0.18	0.25	0.486	0.64	HIIH
0148+2124	0.0169	4	86	35	103	150	3.64	12.60	0.16	−0.54	0.174	0.37	BCD
0150+2032	0.0323	6	140	89	329	400	1.09	3.42	−0.32	−0.17	0.085	3.02	HIIH
b	0.0322	12	57	16	24	87	0.32	1.37	−0.06	−0.01	0.357	0.86	HIIH
0156+2410	0.0134	32	6	6	12	47	0.12	0.74	0.03	...	0.702	0.41	DANS
0157+2102	0.0106	31	49	10	36	67	2.91	14.00	−0.17	0.08	0.474	0.42	HIIH
0157+2413	0.0177	13	26	7	35	52	0.19	1.19	0.54	0.81	0.725	1.82	Sy2
0159+2354	0.0170	9	31	9	15	74	0.26	1.37	0.63	−0.28	0.565	0.27	HIIH
0159+2326	0.0178	32	0	0	0	40	0.00	1.75	0.47	0.42	...	0.53	DANS
1246+2727	0.0199	7	60	7	23	78	0.51	3.44	−0.14	−0.11	0.775	1.53	HIIH
1247+2701	0.0231	18	0	4	4	31	0.13	0.64	...	...	0.515	0.22	DANS
1248+2912	0.0217	15	0	4	0	43	0.12	0.74	0.12	0.17	0.715	1.04	SBN
1253+2756	0.0165	6	57	22	27	155	3.39	9.25	−0.10	−0.29	...	1.13	HIIH
1254+2740	0.0172	16	46	7	8	57	0.61	3.56	0.21	0.28	0.645	0.81	SBN
1254+2802	0.0253	4	0	0	0	16	0.00	0.98	0.33	0.22	...	0.17	DANS
1255+2734	0.0234	12	0	16	22	121	0.38	2.36	0.32	0.34	0.715	0.80	SBN
1255+2819	0.0273	18	...	6	2	63	0.32	1.87	...	0.05	0.651	1.48	SBN
1255+3125	0.0258	19	68	15	45	74	1.54	6.90	0.29	0.42	0.409	1.45	HIIH
1256+2701	0.0247	2	...	37	63	118	0.41	1.51	...	−0.45	0.220	0.64	HIIH
1256+2717	0.0273	10	46	11	40	68	0.19	0.89	0.02	0.08	0.447	0.23	DHIIH
1256+2722	0.0287	16	11	4	0	37	0.48	3.78	0.39	0.64	0.928	3.78	DANS
1256+2732	0.0234	23	37	14	12	114	1.30	7.90	−0.06	0.10	...	1.30	SBN
1256+2754	0.0172	26	0	6	2	66	0.51	2.96	0.50	0.10	0.645	0.82	SBN
1256+2823	0.0307	12	0	12	0	109	0.67	3.86	−0.04	0.28	0.644	2.82	SBN
1256+2910	0.0279	17	0	0	0	23	0.00	0.45	...	0.19	...	...	SBN
1257+2808	0.0181	22	7	2	2	42	0.11	1.41	0.07	0.24	1.344:	0.29	SBN
1258+2754	0.0253	4	27	6	6	129	0.34	2.94	−0.11	−0.25	1.020:	1.73	SBN
1259+2755	0.0235	28	10	5	1	62	0.81	6.32	0.09	0.25	0.913	1.81	SBN
1259+2934	0.0239	6	68	28	75	277	1.12	9.42	...	0.36	0.984	8.76	Sy2
1259+3011	0.0307	28	...	3	7	34	0.28	1.68	...	0.01	0.682	0.75	SBN
1300+2907	0.0219	12	0	21	74	106	0.31	1.72	0.08	−0.14	0.620	1.38	HIIH
1301+2904	0.0266	13	0	15	19	81	1.23	4.42	...	−0.31	0.207	1.51	HIIH
1302+2853	0.0237	18	35	6	9	48	0.56	3.14	−0.05	0.01	0.621	0.43	DHIIH
1302+3032	0.0342	16	30	7	22	53	0.76	4.15	−0.11	0.12	0.595	1.26	HIIH
1303+2908	0.0261	3	86	29	131	175	1.84	5.15	...	−0.31	...	1.20	HIIH
1304+2808	0.0210	13	...	7	5	33	0.61	1.98	...	0.02	0.114	0.55	SBN
1304+2818	0.0244	2	0	23	0	115	0.41	1.33	0.27	−0.09	0.111:	2.31	SBN
1304+2830	0.0217	8	58	11	22	67	0.16	0.70	0.20	0.09	0.372	0.08	DHIIH
1306+2938	0.0211	7	32	10	8	133	1.32	6.53	...	−0.12	0.501	2.11	SBN
1306+3111	0.0168	4	29	9	0	81	0.48	3.97	0.29	0.01	...	0.53	DANS
1307+2910	0.0183	21	35	3	1	39	0.27	2.22	0.31	0.52	0.970	2.56	SBN
1308+2950	0.0246	13	18	5	0	59	0.29	3.78	0.66	0.85	1.381:	3.08	SBN

Table 5. continued

UCM	z	SNR	EW(Å)				Flux*		$b-v$	$v-r$	E_{B-V}	$L_{H\alpha}$	Spect
			[OII]	Hβ	[OIII]	Hα†	Hβ	Hα				$10^8\ L_\odot$	Type
1308+2958	0.0223	15	0	2	0	26	0.10	1.23	0.28	0.40	1.313:	7.03	SBN
1310+3027	0.0234	5	0	0	0	70	0.00	2.36	0.70	0.48	...	0.63	DANS
1312+2954	0.0230	4	0	7	8	65	0.24	2.24	0.53	0.21	1.087:	0.96	SBN
1312+3040	0.0210	8	0	9	9	81	0.54	2.60	0.42	0.16	0.474	1.51	SBN
1313+2938	0.0380	27	...	54	212	353	3.24	8.16	...	−0.06	...	4.36	HIIH
1314+2827	0.0253	21	18	6	6	65	0.41	2.67	0.07	0.03	0.749	0.80	SBN
1320+2727	0.0247	10	...	11	30	61	0.13	0.47	...	−0.31	0.205	0.23	DHIIH
1324+2650	0.0249	29	11	12	14	101	2.02	11.50	−0.12	0.19	0.628	3.75	SBN
1324+2926	0.0172	7	132	50	320	251	2.01	5.89	0.19	0.07	0.022	0.36	BCD
1331+2900	0.0356	7	74	136	1144	573	1.13	3.28	...	0.05	0.013	0.61	BCD
1428+2727	0.0149	15	95	39	159	218	5.10	17.20	...	−0.21	0.150	2.35	HIIH
1429+2645	0.0328	20	...	20	56	96	0.68	2.18	...	−0.29	0.105	0.55	DHIIH
1430+2947	0.0290	10	...	27	72	156	1.85	7.42	0.18	0.21	0.308	1.59	HIIH
1431+2702	0.0384	7	52	24	35	180	1.21	4.66	0.01	0.08	0.271	2.05	HIIH
1431+2814	0.0320	17	0	0	0	17	0.00	0.85	0.60	0.28	...	0.27	DANS
1431+2854	0.0310	8	5	0	0	24	0.00	0.97	0.46	0.17	...	0.89	SBN
1431+2947	0.0219	4	87	29	286	136	0.69	1.94	0.07	−0.16	...	0.21	BCD
1432+2645	0.0307	15	0	4	4	47	0.32	2.50	0.14	0.28	0.914	2.09	SBN
1440+2511	0.0333	16	0	3	2	35	0.10	0.87	0.49	0.47	1.018:	0.57	SBN
1440+2521N	0.0315	7	53	9	14	104	0.38	2.54	0.66	0.09	0.773	1.59	SBN
1440+2521S	0.0314	4	40	17	28	100	0.71	2.78	0.23	−0.02	0.292	1.04	SBN
1442+2845	0.0110	9	22	10	0	135	1.02	6.15	0.36	−0.01	0.681	0.66	SBN
1443+2548	0.0351	17	0	9	5	76	0.62	3.92	0.19	0.35	0.726	2.63	SBN
1443+2714	0.0290	16	29	13	115	149	1.17	10.10	0.45	0.34	1.008	4.60	Sy2
1443+2844	0.0279	7	27	0	0	75	0.00	6.86	0.29	0.15	...	1.99	SBN
1444+2923	0.0281	11	24	3	0	29	0.14	0.91	0.36	0.16	0.785:	0.37	DANS
1452+2754	0.0339	15	18	4	3	135	0.48	3.05	0.45	0.36	0.733	3.09	SBN
1506+1924	0.0205	4	52	12	23	140	0.69	0.33	0.26	0.03	0.453	1.95	HIIH
1513+2012	0.0369	15	37	18	21	150	2.30	11.90	0.21	0.36	0.540	6.18	SBN
1537+2506N	0.0231	3	137	38	120	200	1.85	6.77	0.05	0.17	0.225	5.35	HIIH
1537+2506S	0.0231	7	17	26	15	201	3.10	13.10	0.24	0.11	0.357	1.88	HIIH
1557+1423	0.0275	31	...	10	5	54	0.65	2.82	...	0.22	0.374	0.64	SBN
1612+1308	0.0114	18	110	94	464	550	1.62	4.80	−0.31	−0.22	0.031	0.15	BCD
1646+2725	0.0339	14	...	41	155	225	0.81	3.19	...	−0.05	0.288	0.50	DHIIH
1647+2727	0.0369	37	30	9	9	79	0.39	2.36	0.08	0.35	0.678	1.03	SBN
1647+2729	0.0366	23	14	6	4	59	0.50	3.80	0.15	0.41	0.895	2.06	SBN
1647+2950	0.0290	10	14	11	12	110	1.07	6.86	0.18	0.17	0.736	3.76	SBN
1648+2855	0.0308	3	88	24	35	240	0.92	3.46	−0.13	−0.11	0.247	6.23	HIIH
1653+2644	0.0393	35	0	0	0	5	0.00	1.80	0.41	0.44	...	0.87	SBN
1654+2812	0.0348	4	54	15	43	70	0.15	0.61	0.28	0.25	0.313	0.33	DHIIH
1655+2755	0.0349	17	62	11	120	81	0.76	4.10	0.59	0.73	0.583	4.66	Sy2
1656+2744	0.0330	33	19	12	13	108	0.64	3.42	0.13	0.38	0.578	1.08	SBN
1657+2901	0.0317	15	0	10	5	80	0.49	2.57	...	...	0.561	0.68	DANS
1659+2928	0.0369	3	58	13	16	217	0.47	2.41	0.25	0.40	0.528:	8.80	Sy1
1701+3131	0.0345	23	19	2	6	121	0.41	9.41	0.10	0.36	1.904:	7.23	Sy1
2238+2308	0.0240	34	11	6	0	69	1.68	15.20	0.14	0.33	1.051	3.15	SBN
2239+1959	0.0258	7	50	22	97	173	5.20	26.80	0.04	0.15	0.537	5.00	HIIH
a	0.0258	10	54	12	9	116	0.53	3.36	0.04	0.15	0.732	5.00	HIIH
2249+2149	0.0462	15	0	0	0	4	0.00	0.43	0.64	0.61	...	...	SBN

Table 5. continued

UCM	z	SNR	EW(Å)				Flux*		$b-v$	$v-r$	E_{B-V}	$L_{\mathrm{H}\alpha}$	Spect
			[OII]	Hβ	[OIII]	Hα†	Hβ	Hα				$10^8\ L_\odot$	Type
2250+2427	0.0429	34	2	10	4	165	1.62	10.80	−0.19	0.10	0.773	10.69	SBN
a	0.0427	8	36	15	11	175	0.28	1.73	−0.03	0.32	0.709	11.12	SBN
2251+2352	0.0267	15	28	15	20	84	0.28	0.98	−0.01	...	0.184	0.97	DANS
2253+2219	0.0242	21	0	11	8	86	0.13	0.67	0.05	...	0.537	1.07	SBN
2255+1654	0.0388	38	19	1	2	40	0.02	0.23	0.52	...	1.473	1.39	SBN
2255+1926	0.0193	23	27	6	19	37	0.52	2.24	−0.07	0.10	0.366	0.16	HIIH
2255+1930N	0.0198	19	30	14	11	97	0.74	4.53	0.31	0.38	0.699	1.38	SBN
2255+1930S	0.0203	24	34	9	16	61	0.85	4.19	0.08	0.17	0.493	0.52	SBN
2256+2001	0.0242	9	0	0	0	15	0.00	1.40	0.64	0.35	...	0.42	DANS
2257+1606	0.0339	22	13	3	9	32	0.34	2.37	0.33	0.42	0.807:	...	SBN
2257+2438	0.0345	11	20	66	88	365	0.76	15.50	0.03	0.26	0.540	4.67	Sy1
2258+1920	0.0220	19	0	12	20	190	1.10	4.61	0.70	0.11	0.348	1.75	DANS
2300+2015	0.0346	31	...	27	113	159	0.47	1.93	0.41	0.46	0.326	3.17	SBN
2302+2053E	0.0328	11	9	3	0	36	0.27	3.19	0.02	0.31	1.301	1.68	SBN
2302+2053W	0.0328	30	73	42	59	260	0.83	3.92	0.46	0.47	0.457:	1.38	HIIH
2303+1702	0.0428	3	23	6	58	185	0.05	1.72	0.18	...	0.416	3.19	Sy2
2303+1856	0.0276	18	12	7	6	79	0.50	5.31	0.43	0.53	1.199:	2.41	SBN
2304+1640	0.0179	13	67	27	117	155	0.47	1.93	−0.16	−0.05	0.333	0.20	BCD
2304+1621	0.0384	10	63	12	5	63	0.03	1.15	0.40	...	0.397	2.04	DANS
2307+1947	0.0271	31	7	6	9	45	0.10	0.46	0.25	...	0.453	0.64	DANS
2307+2119	0.0000	12	0	91	0	75	2.71	4.85	...	0.92	...	...	Simb
2310+1800	0.0363	19	...	7	2	63	0.24	1.84	0.62	0.62	0.904	1.46	SBN
2312+2204	0.0327	21	20	7	6	63	0.37	2.69	0.32	0.24	0.864	1.35	SBN
2313+1841	0.0300	8	0	9	4	82	0.61	4.76	0.63	...	0.914	0.72	SBN
2313+2517	0.0273	28	0	0	7	47	0.00	10.90	0.45	0.38	...	4.11	SBN
a	0.0273	33	0	2	9	48	0.57	7.88	0.54	0.42	1.437	4.19	SBN
2315+1923	0.0385	25	67	35	80	190	0.59	2.91	0.57	0.65	0.495	1.49	HIIH
2316+2028	0.0263	5	73	14	25	99	0.55	3.60	...	...	0.755	0.49	DANS
2316+2457	0.0277	42	0	4	0	57	1.84	19.00	0.24	0.28	1.172:	5.83	SBN
a	0.0277	18	20	13	9	109	1.10	6.72	0.10	0.38	0.693	10.58	SBN
b	0.0277	34	14	4	0	50	3.00	51.00	0.19	0.33	1.626:	5.15	SBN
c	0.0277	15	0	0	0	69	0.00	5.05	0.14	0.21	...	6.97	SBN
2316+2459	0.0274	19	0	7	0	52	0.50	3.81	0.36	0.21	0.894:	10.53	SBN
a	0.0274	6	0	0	0	42	0.00	0.33	0.37	0.29	...	1.02	SBN
b	0.0274	9	0	0	0	54	0.00	0.63	0.24	0.28	...	1.30	SBN
c	0.0274	15	0	0	0	61	0.00	1.64	0.19	0.16	...	1.46	SBN
d	0.0274	13	0	16	7	72	0.24	1.28	0.19	0.16	0.568:	10.16	SBN
2317+2356	0.0334	49	0	0	0	29	0.00	19.80	0.26	0.30	...	5.59	SBN
a	0.0334	34	0	0	0	11	0.00	1.78	0.40	0.20	...	2.16	LINER
b	0.0334	17	20	20	8	128	1.10	7.00	−0.04	0.09	...	22.31	SBN
2319+2234	0.0364	25	24	18	8	108	0.79	4.31	0.21	0.41	0.588	1.91	SBN
2319+2243	0.0313	18	30	0	9	33	0.00	3.97	0.39	0.20	...	1.34	SBN
2320+2428	0.0328	34	0	0	0	7	0.00	1.15	0.63	0.47	...	0.42	DANS
2321+2149	0.0374	16	38	9	6	68	0.52	2.75	0.08	0.21	0.559	1.38	SBN
2321+2506	0.0331	21	32	2	3	60	0.36	8.00	0.14	0.13	...	1.65	SBN
2322+2218	0.0249	21	0	22	0	64	0.15	0.90	...	...	0.676	0.32	SBN
2324+2448	0.0123	46	0	1	0	10	0.09	0.11	0.50	0.43	1.300	1.20	SBN
2325+2318	0.0122	40	49	13	31	101	9.02	45.10	−0.02	−0.08	...	3.18	HIIH
b	0.0105	25	31	8	26	92	2.31	8.97	−0.19	−0.30	...	2.16	HIIH
c	0.0108	20	89	53	120	440	11.40	43.20	−0.29	−0.33	...	8.11	HIIH

Table 5. continued

UCM	z	SNR	EW(Å)				Flux*		$b-v$	$v-r$	E_{B-V}	$L_{H\alpha}$	Spect
			[OII]	Hβ	[OIII]	Hα†	Hβ	Hα				$10^8\ L_\odot$	Type
2325+2208	0.0130	20	30	27	11	237	4.72	22.00	−0.18	−0.01	...	15.73	SBN
b	0.0130	47	0	4	0	49	1.26	12.10	0.39	0.31	1.105:	3.90	SBN
c	0.0145	10	0	0	0	68	0.00	1.85	0.10	−0.25	...	6.59	SBN
2326+2435	0.0174	11	98	40	192	224	1.39	5.39	−0.04	0.12	0.278	0.83	DHIIH
2327+2515N	0.0206	8	99	44	176	289	4.84	23.30	−0.15	0.03	0.474	1.83	HIIH
2327+2515S	0.0206	14	46	16	49	104	1.81	7.71	−0.22	−0.02	0.364	1.07	HIIH
2329+2427	0.0200	23	0	0	0	17	0.00	1.37	0.66	0.51	...	0.30	DANS
2329+2500	0.0305	29	6	46	32	230	2.07	7.70	0.24	0.42	...	5.00	Sy1
2329+2512	0.0133	22	38	10	48	60	0.89	4.18	0.06	0.04	0.453	0.13	DHIIH
2331+2214	0.0352	28	29	8	9	79	0.30	2.28	0.36	0.31	0.892	0.81	SBN
2333+2248	0.0399	36	0	35	103	201	2.12	9.22	...	0.24	0.383	2.52	HIIH
2333+2359	0.0395	21	...	32	18	111	3.13	11.10	...	0.14	0.197	2.42	Sy1
2348+2407	0.0359	17	29	10	6	72	0.57	2.86	0.07	0.42	0.517	0.89	SBN
2351+2321	0.0273	14	0	22	48	117	1.49	3.32	...	...	...	0.73	HIIH

Hα luminosities are similar to those of SBN class. The observed [OIII] λ5007 / Hβ and Hα / [NII] λ6584 are large. As examples we can cite UCM 0150+2032 or UCM 1301+2904.

DHIIH. This is a HIIH subclass with spectroscopic properties similar to those of HIIH class except Hα luminosities lower than 5 $10^7\ L_\odot$. In average, they present lower color excess.

BCD. The objects with lowest luminosity and highest ionization have been classified as Blue Compact Dwarf galaxies. It is difficult to characterize properly this kind of galaxies and several definitions can be found in the literature. Due to the spectroscopic nature of this work, we will emphasize the spectral properties. The BCD class is characterized by low Hα luminosities ($\leq 5\ 10^7\ L_\odot$), high excitation emission lines, Helium lines present, strong [OIII] lines and equivalent widths in the order of several hundred angstroms. The [OIII] λ5007 / Hβ ratio is high, the [NII] λλ6548 and 6584 lines are usually weak or even not detected and [OII] λ3727 is also usually weak. The BCDs are faint galaxies that become visible when they experience an strong starburst that dominates the total energy output. The most representative object in the UCM sample is UCM 1612+1308.

6. Summary

We have obtained spectra for essentially all ELG candidates in lists 1 and 2 of the UCM survey. In the present paper we have detailed our observational and reduction procedures, and presented the data. Our spectra provide important redshift information, plus optical reddening estimates, line fluxes and equivalent widths which are fundamental to understanding the physical processes occurring in these star forming objects. We have concluded that the assigned value of equivalent width parameter correlates with the observed data, but the large overlap in these quantities reduces their usefulness for predicting true line fluxes. The UCM emission-line galaxies have been classified by their spectra according to different natural spectroscopic groups.

These data will be used in succeeding papers to study the physical properties of the UCM ELGs and the completeness of the survey along with the luminosity and spatial distributions of the ELGs.

Acknowledgements. This work was supported in part by the Spanish "Programa Sectorial de Promoción del Conocimiento" under grants PB89–124 and PB93–456.

A. Spectroscopic data

This appendix is devoted to a presentation of plots of the spectra for all the UCM emission-line galaxies with an spectroscopic image of enough quality. For each object gray-scale frames of the CCD images at the regions near Hβ λ4861 and Hα λ6563 are given. Each panel also includes the individual spectra and the spatial profiles at both the emission line and the adjacent continuum for the two regions previously mentioned. The identification label lists the UCM name with a letter for the different nodes from east to west and the spectroscopic type assigned. The spectra are unsmoothed and plot F_λ (10^{-15} erg s^{-1} cm^{-2} Å^{-1} units) against wavelength (Å).

References

Acker A., Ochsenbein F., Stenholm B., Tylenda R., Marcout J., Schohn C., 1992, The Strasbourg-ESO catalogue of Galactic Planetary Nebulae, ESO edit. Germany
Balzano V.A., 1983, ApJ 268, 602

Table 6. a) Candidates with no emission

UCM 0009+2024	UCM 0012+2109	UCM 0009+2045	UCM 0036+2007
UCM 0038+0235	UCM 0043+2440	UCM 0045+2256	UCM 0045−0157
UCM 0049+0013	UCM 0053+2352	UCM 0130+2505	UCM 0138+2016
UCM 0142+2441	UCM 0150+2056	UCM 0152+2039	UCM 1253+2926
UCM 1254+2932	UCM 1254+2741	UCM 1254+2853	UCM 1257+2825
UCM 1300+3136	UCM 1300+2959	UCM 1306+3100	UCM 1310+2737
UCM 1321+2648	UCM 1439+2439	UCM 1441+2918	UCM 1445+2855
UCM 1449+2844	UCM 1451+2954	UCM 1604+1642	UCM 1651+3017
UCM 2244+2049	UCM 2306+1703	UCM 2328+2109	UCM 2333+2241
UCM 2346+2011	UCM 2352+2040	UCM 2358+2327	

Table 6. b) Confirmed stars

UCM 0001+2024	UCM 0038+2302	UCM 0138+2047	UCM 1309+2936
UCM 1325+2955	UCM 1330+3011	UCM 1536+2338	UCM 1608+1335
UCM 1651+2721	UCM 2239+2402	UCM 2251+2405	UCM 2253+2453
UCM 2315+1658	UCM 2320+2036	UCM 2322+2204	UCM 2323+2047
UCM 2323+2252	UCM 2327+2154	UCM 2327+1956	UCM 2329+2447
UCM 2334+2134	UCM 2344+2157	UCM 2352+2230	UCM 2353+2027
UCM 2354+2232	UCM 2357+2440	UCM 2357+2241	

Table 6. c) Confirmed galaxies with no emission

UCM	z	EW (Å) Hα+[NII]	$b-v$	$v-r$
UCM 0053−0049	0.0261	2 ?	0.12	0.09
UCM 0138+2216	0.0591	15 ?	0.84	0.43
UCM 0139+2226	0.0444	4 ?	0.95	0.69
UCM 0155+2507	0.0164	...	...	...
UCM 0157+2324	0.0164	...	...	...
UCM 1304+2848	0.0159	...	...	...
UCM 1447+2535	0.0339	...	...	...
UCM 1449+2847	0.0160	...	...	...
UCM 2241+2431	0.0180	...	...	...
UCM 2312+2500	0.0266	...	...	...

Boksenberg A., 1972, in Auxiliary Instrumentation for large telescopes, Proc. ESO-CERN Conf. 295. In: Lausten S. & Reiz A. (eds.)

Boroson T.A., Salzer J.J., Trotter A., 1993, ApJ 412, 524

Gallego J., Zamorano J., Rego M., Vitores A.G., 1994, A&A 290, 705

Gallego J., 1995, Ph.D. thesis, Universidad Complutense de Madrid

Horne K., 1986, PASP 98, 609

Jenkins C.R., 1986, Spectroscopy with IPCS on the INT Isaac Newton Group User Manual VI

King D.L., 1985, RGO/La Palma Technical Note No. 31.

Markarian B.E., Stepanian J.A., Erastova L.K., 1987, Observational Evidence of Activity in galaxies, IAU Symp. 121. In: Khachikian E. Ye., Fricke K.J. & Melnick J. (eds.). Dordrecht: Reidel, p. 25

Mazzarella J.M., Balzano V.A., 1986, ApJS 62, 751

Oke J.B., 1974, ApJS 27, 21

Oke J.B., Gunn J.E., 1983, ApJ 266, 713

Osterbrock D.E., 1989, Astrophysics of Gaseous Nebulae and Active Galactic Nuclei. University Science Books, U.S.A.

Rego M., Zamorano J., Gallego J., Vitores A., 1994, A&A 281, 348

Rego M., Cordero–Gracia M., Zamorano J., Gallego J., 1993, AJ 105, 427

Rosenberg J.L., Salzer J.J., 1994, AJ 108, 1557

Salzer J.J., MacAlpine G.M., Boroson T.A., 1989, ApJS 70, 447

Salzer J.J., Moody J.W., Rosenberg J.L., Gregory S.A., Newberry M.V., 1995, AJ 109, 2376

Strom K.M., 1977, Kitt Peak National Observatory Memorandum Standard Stars for Intensified Image Dissector Scanner Observations

Vitores A.G., Zamorano J., Rego M., Alonso O., Gallego J., 1996, A&AS 118, 7

Wasilewski A.J., 1983, ApJ 272, 68

Zamorano J., Gallego J., Rego M., Vitores A.G., González–Riestra R., 1992, AJ 104, 1000

Zamorano J., Rego M., Gallego J., et al., 1994, ApJS 95, 387

Zamorano J., Gallego J., Rego M., Vitores A.G., Alonso O., 1996, ApJS 462, 1

UCM0000+2140 HIIH

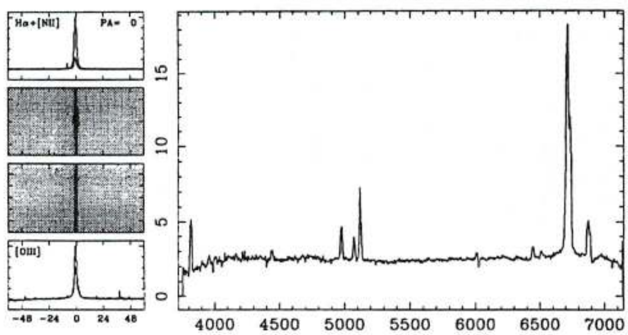

UCM0003+1955 Sy1

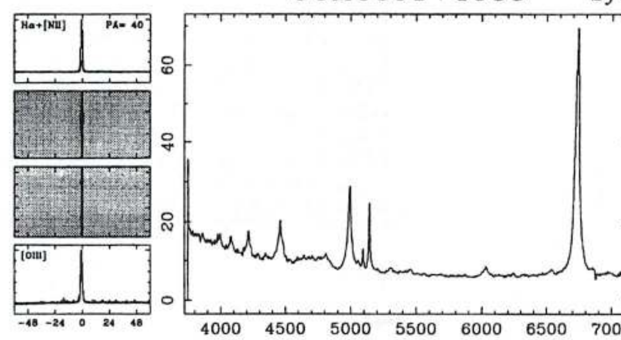

UCM0003+2200 DANS

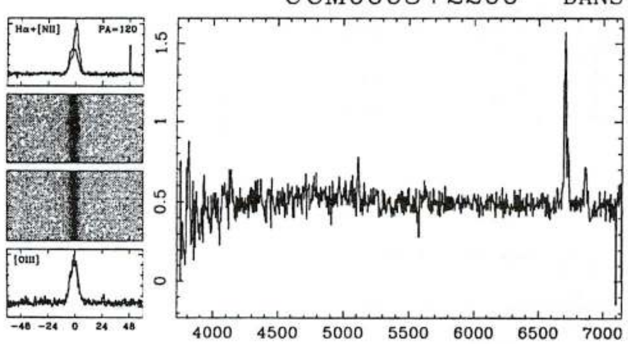

UCM0003+2215 SBN

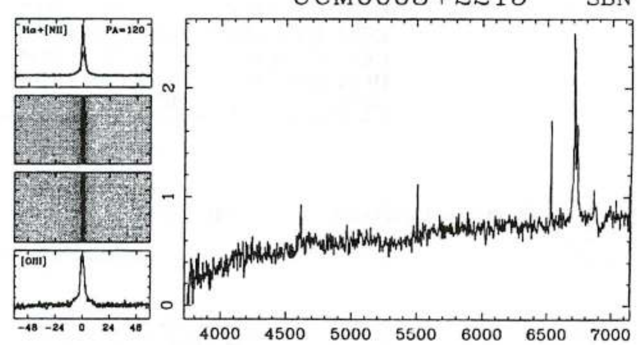

UCM0005+1802 SBN

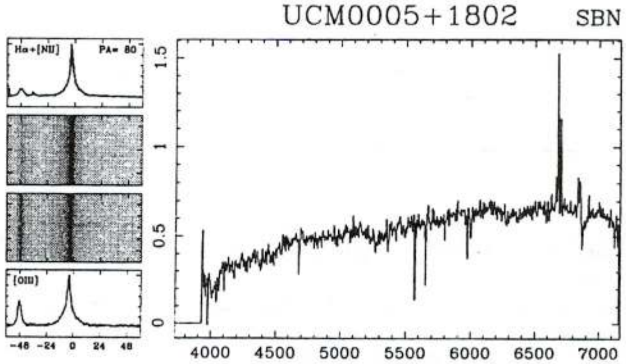

UCM0006+2332 HIIH

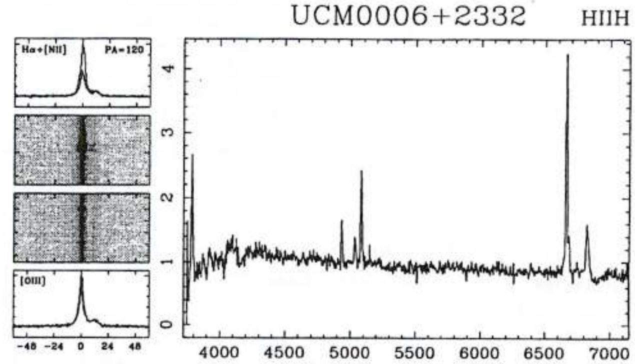

UCM0013+1942 HIIH

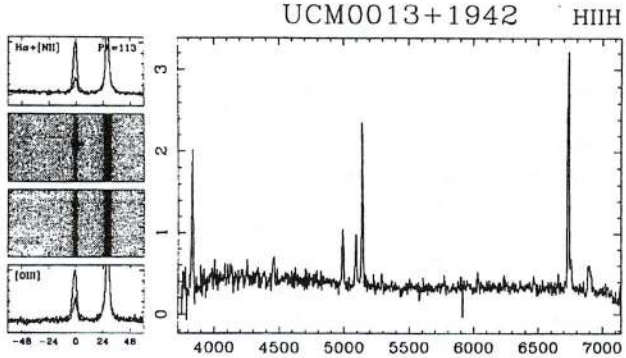

UCM0015+2212 HIIH

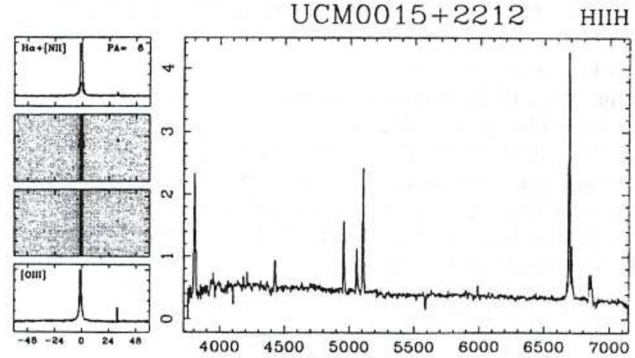

UCM0017+1942 HIIH

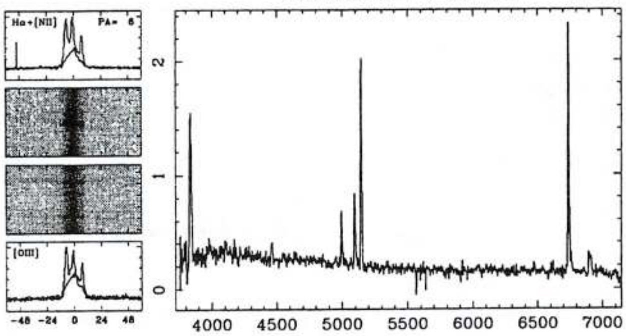

UCM0017+1942b HIIH

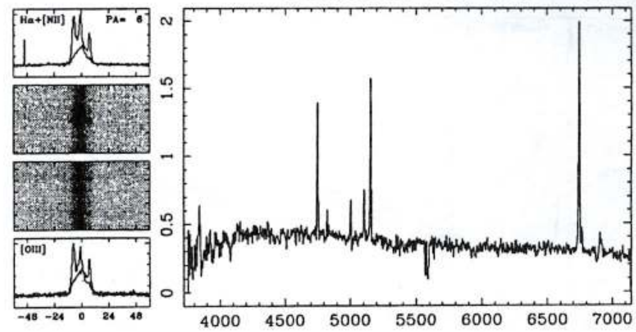

UCM0017+1942c HIIH

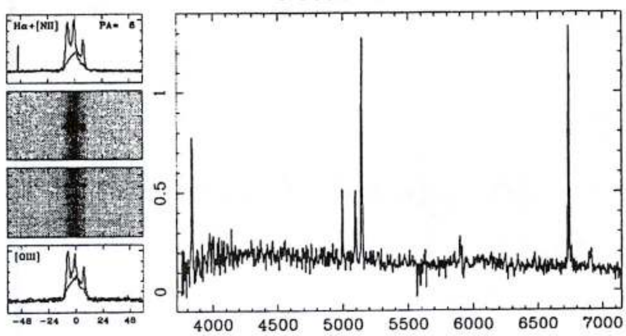

UCM0017+2148 HIIH

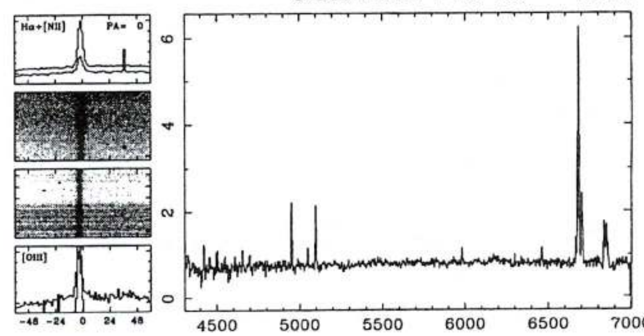

UCM0018+2215 DANS

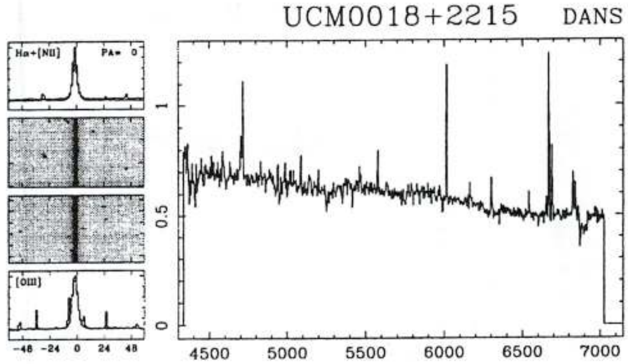

UCM0018+2218 SBN

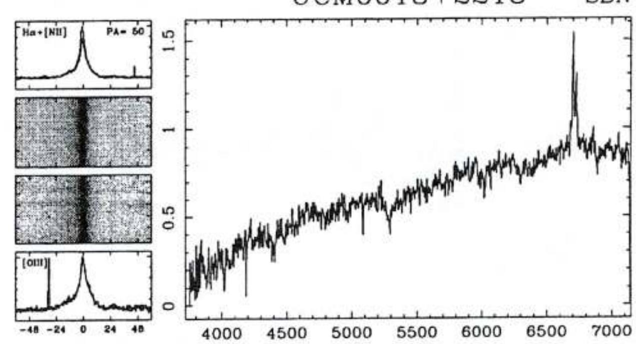

UCM0019+2201 DANS

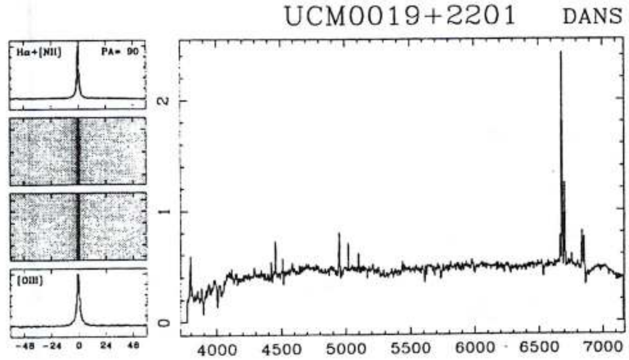

UCM0023+1908 HIIH

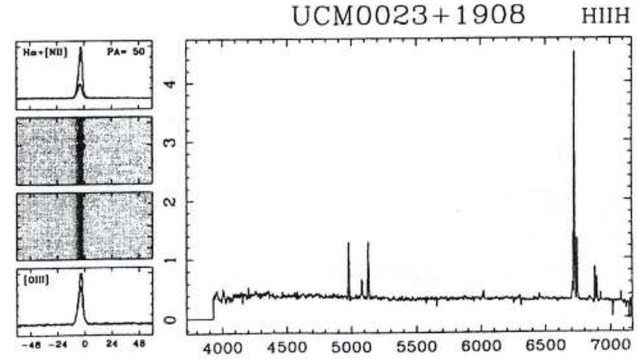

UCM0034+2119 SBN

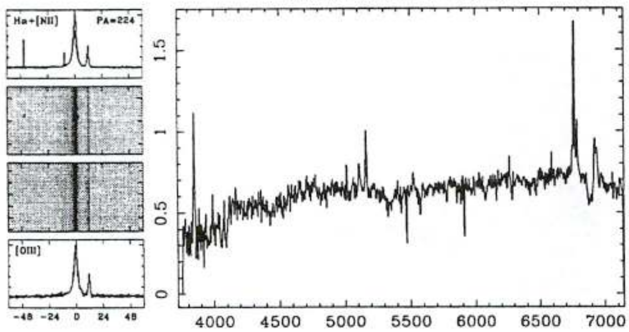

UCM0037+2226 SBN

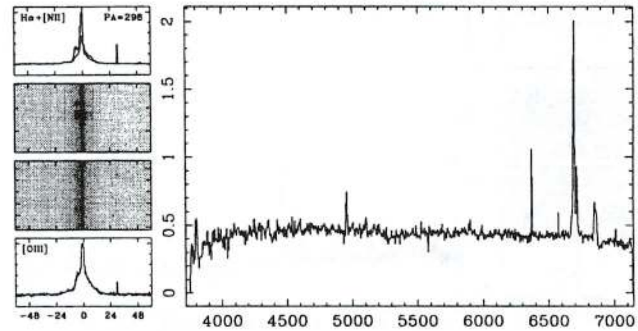

UCM0037+2226a SBN

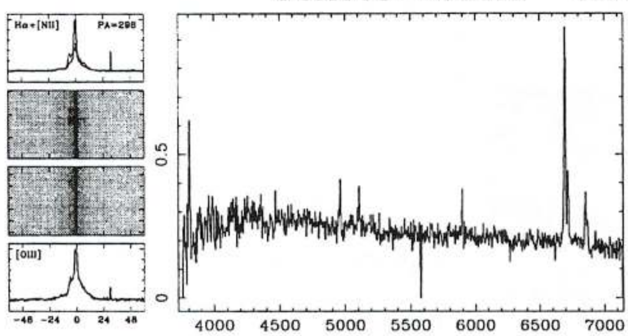

UCM0038+2259 SBN

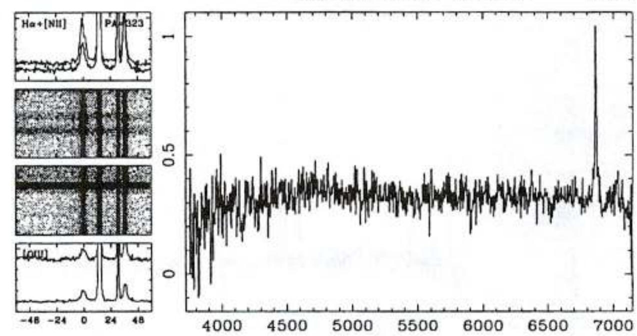

UCM0039+0054 SBN

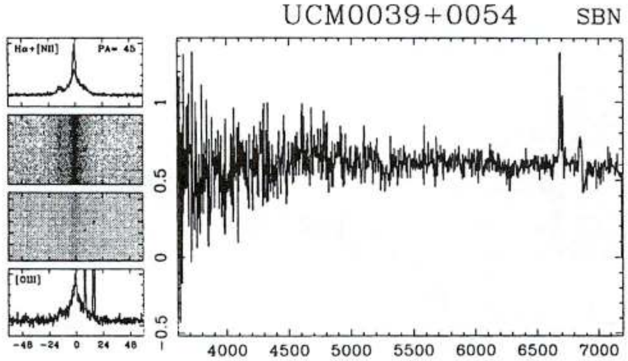

UCM0040−0023 LINER

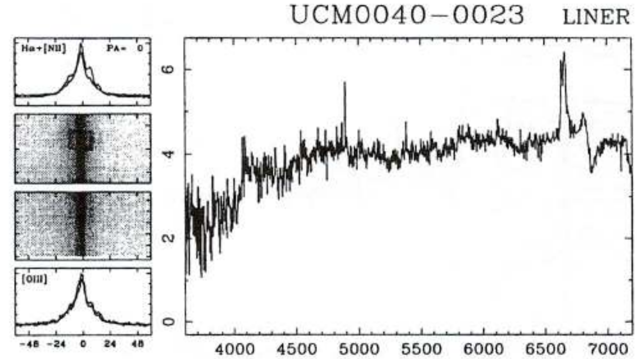

UCM0040+0220 DANS

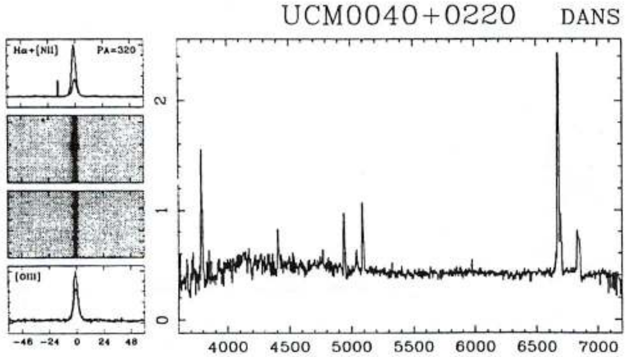

UCM0040+0257 DANS

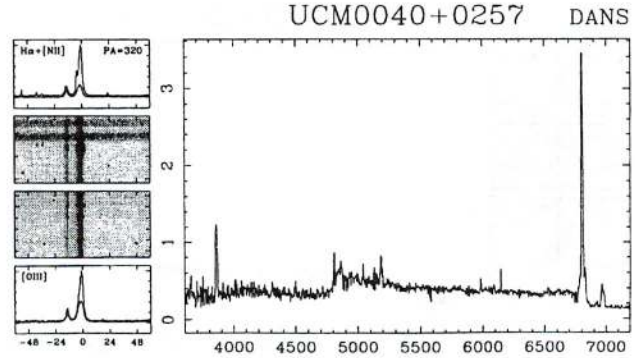

UCM0040+2312 SBN

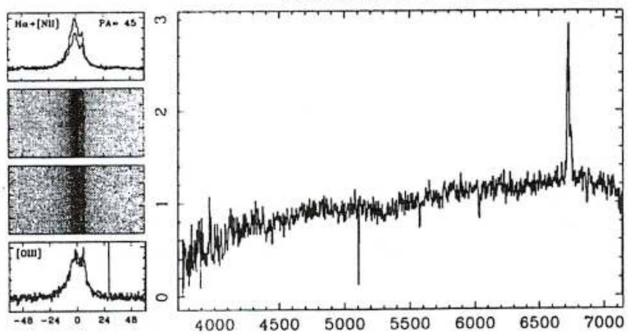

UCM0041+0135 DESC

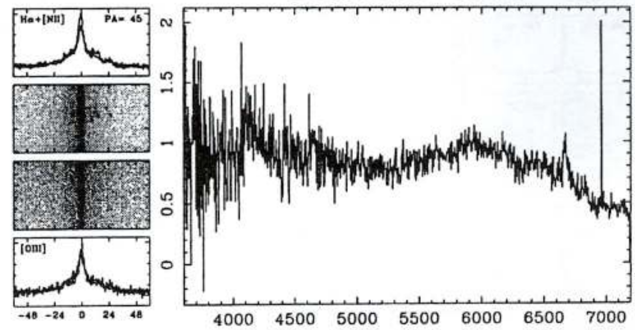

UCM0043−0159 SBN

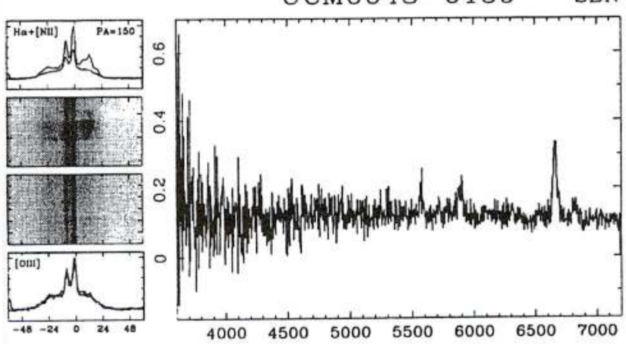

UCM0043+0245 HIIH

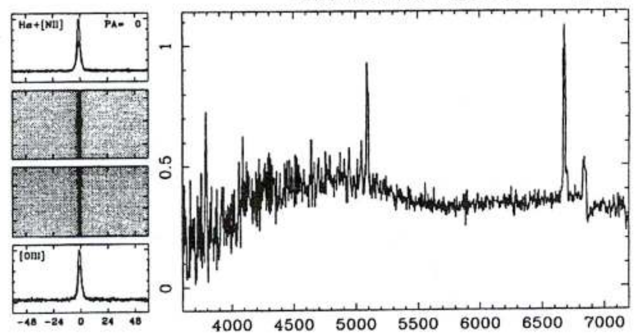

UCM0044+2246 SBN

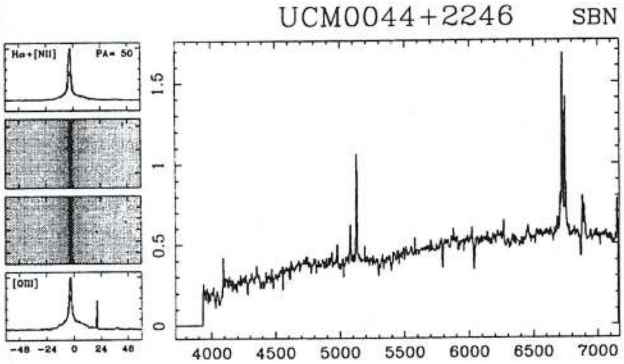

UCM0045+2206 HIIH

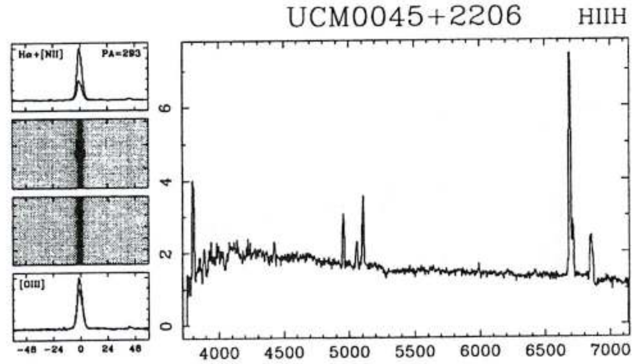

UCM0047−0213 DHIIH

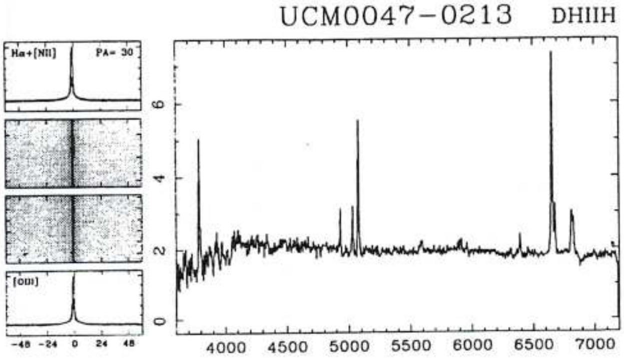

UCM0047+2051 SBN

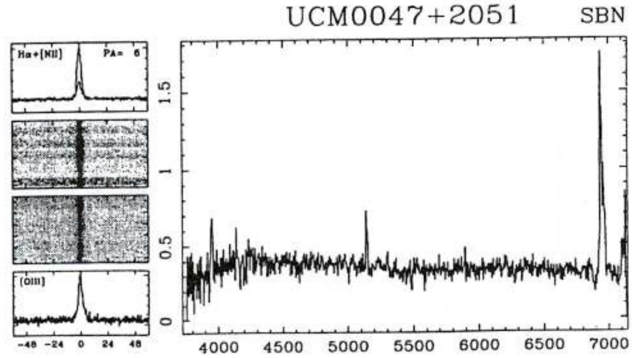

UCM0047+2413 SBN

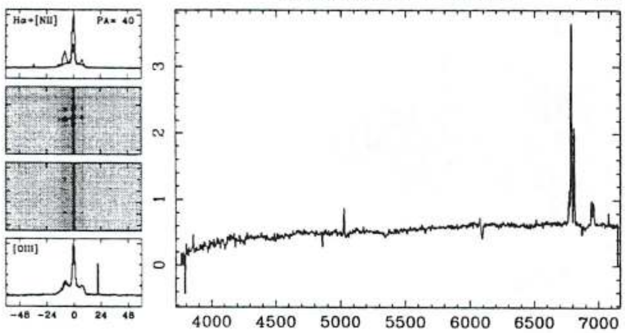

UCM0047+2413a SBN

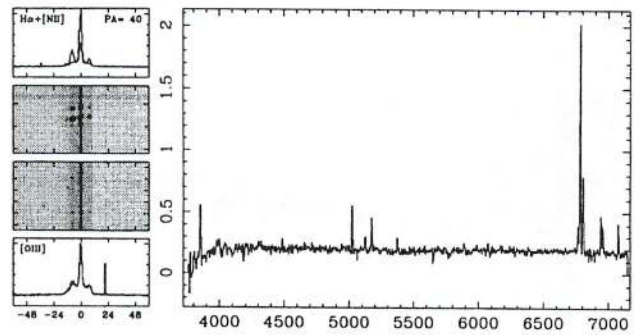

UCM0047+2413c SBN

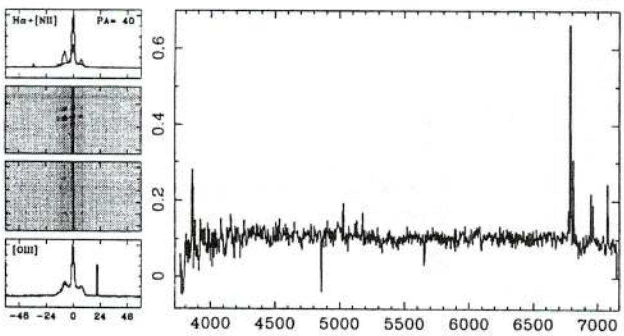

UCM0047+2414 SBN

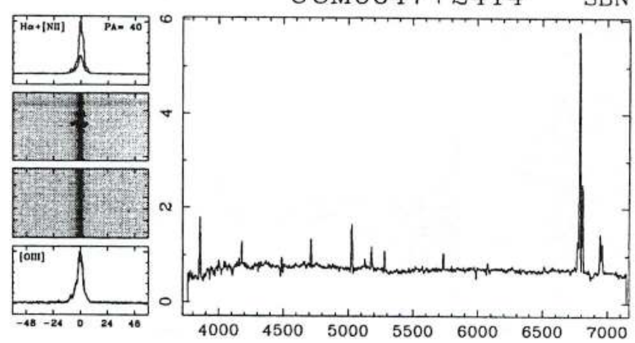

UCM0049−0045a HIIH

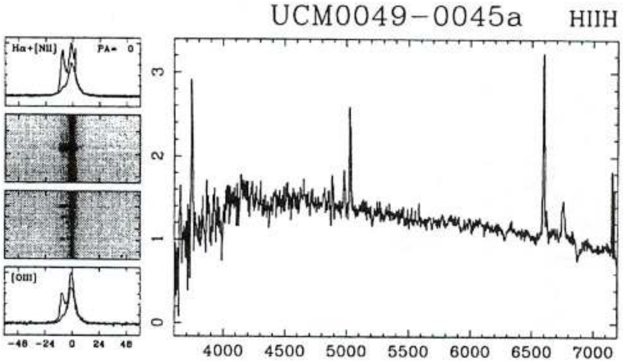

UCM0049−0006 BCD

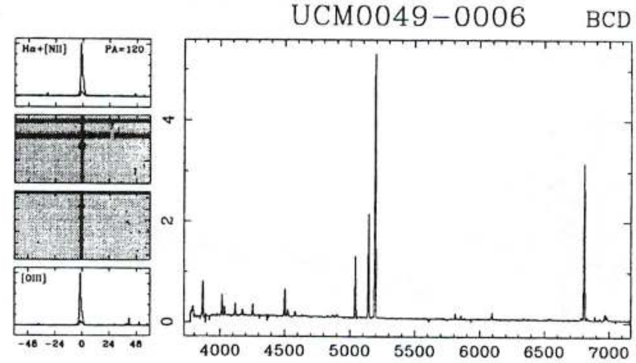

UCM0049+0017 DHIIH

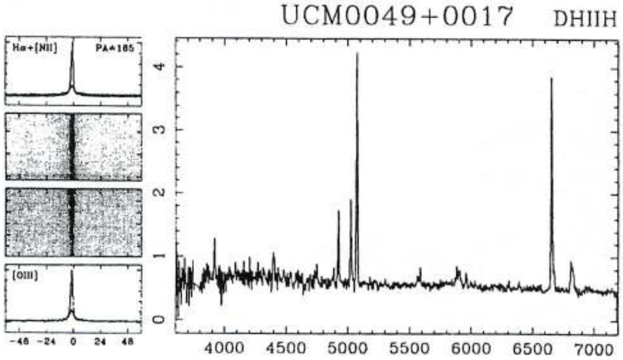

UCM0050+0005 HIIH

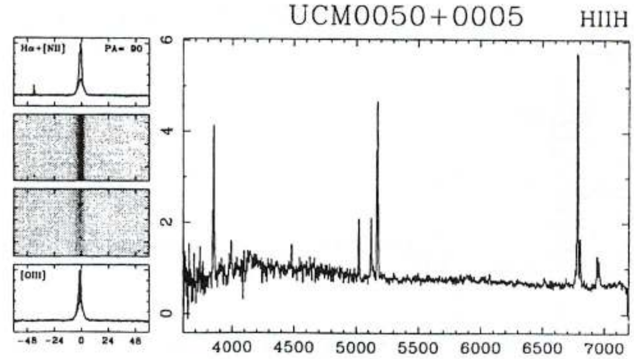

UCM0050+2114 SBN

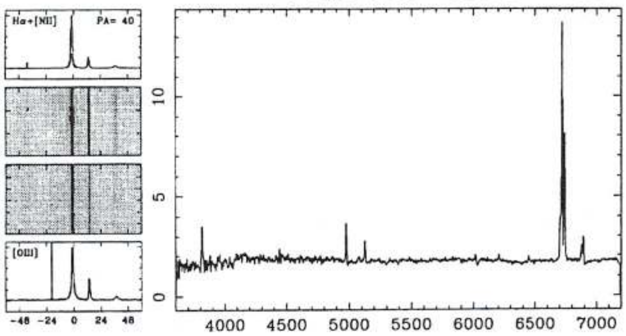

UCM0051+2430 SBN

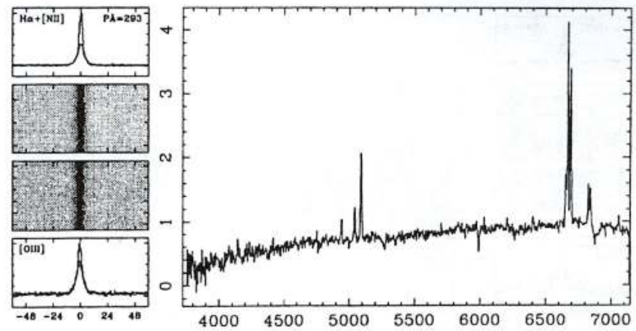

UCM0054−0133 SBN

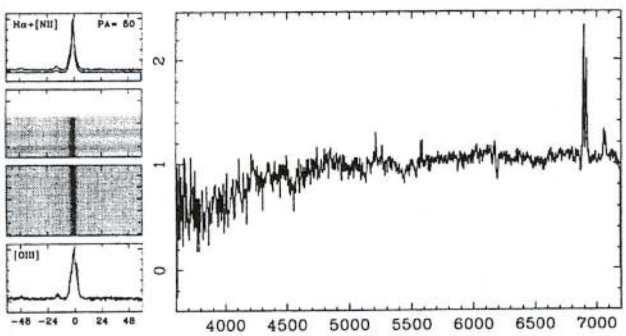

UCM0054+2337 HIIH

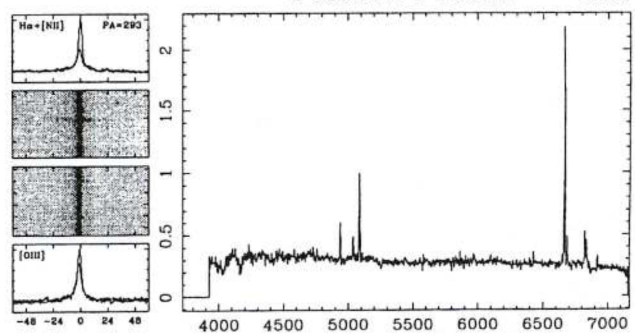

UCM0056+0043 DHIIH

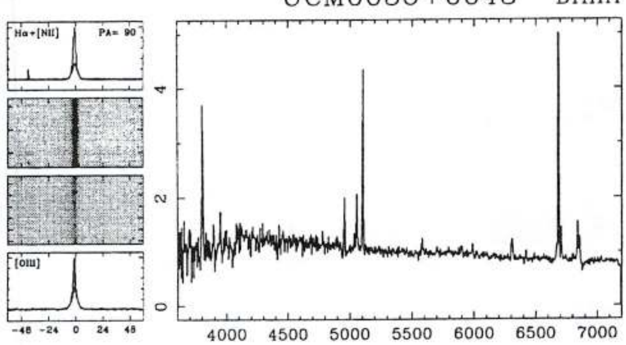

UCM0056+0044 DHIIH

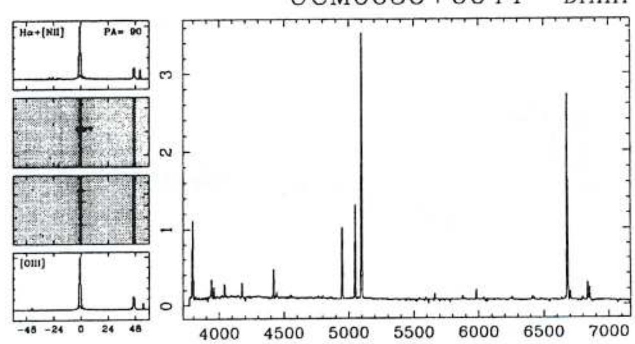

UCM0119+2156 Sy2

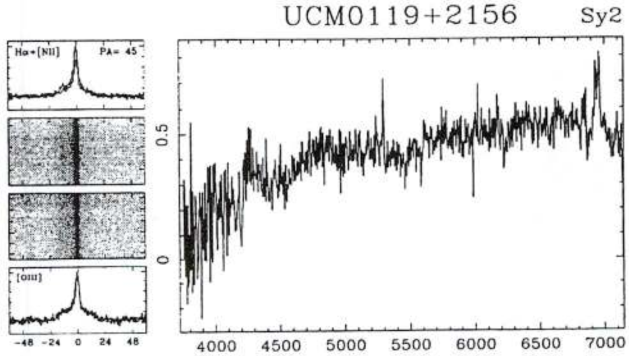

UCM0121+2137 SBN

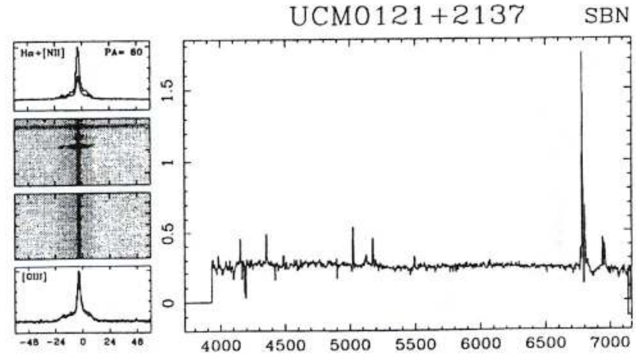

UCM0129+2109 LINER

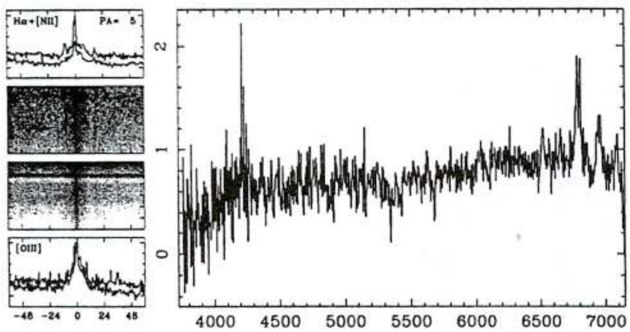

UCM0134+2257 SBN

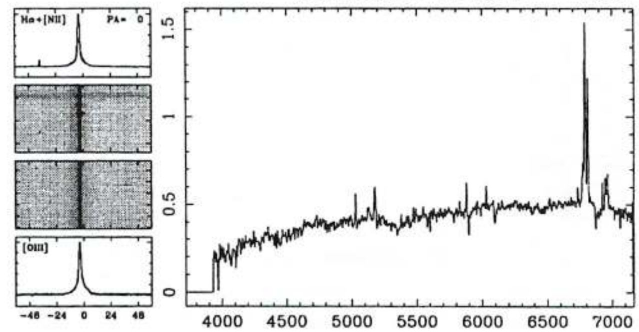

UCM0138+2216 SBN

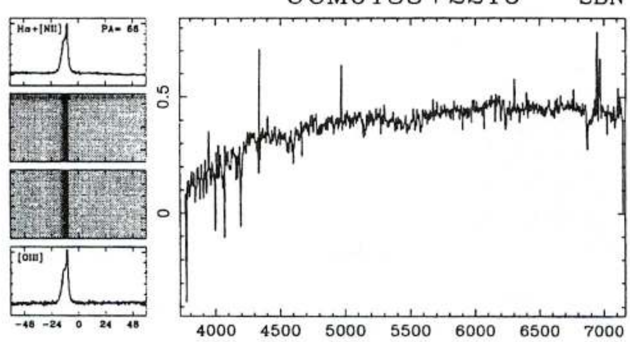

UCM0141+2220 DANS

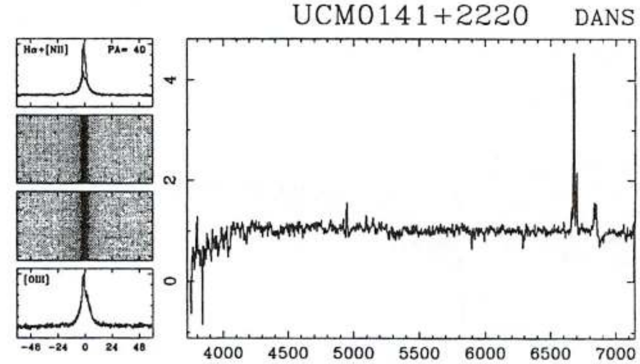

UCM0144+2519 SBN

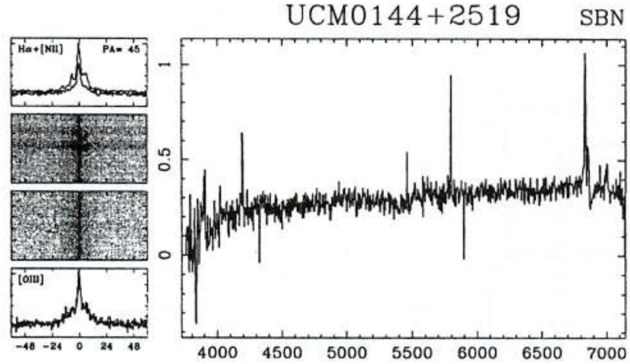

UCM0147+2309 HIIH

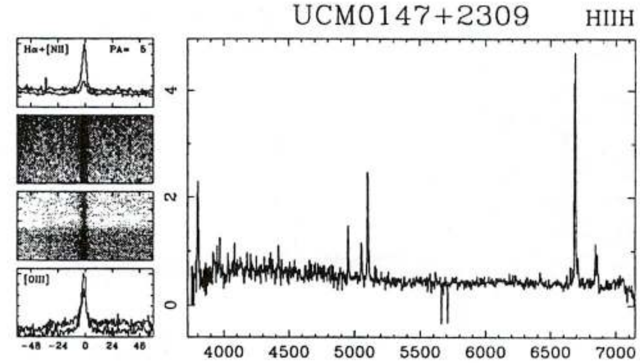

UCM0148+2123 BCD

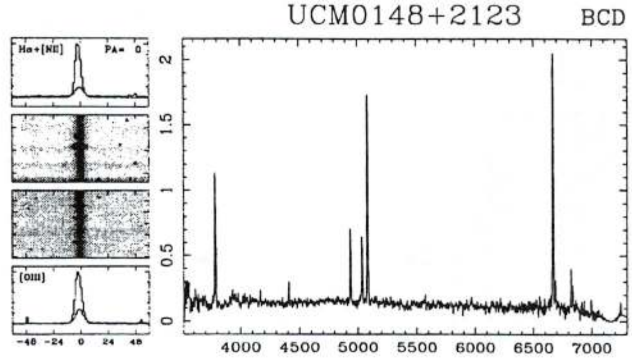

UCM0150+2032 HIIH

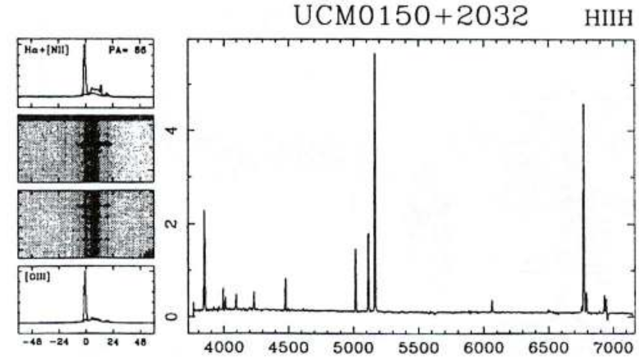

UCM0150+2032b HIIH

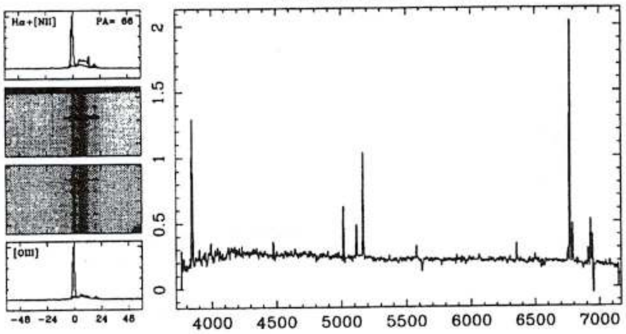

UCM0157+2102 HIIH

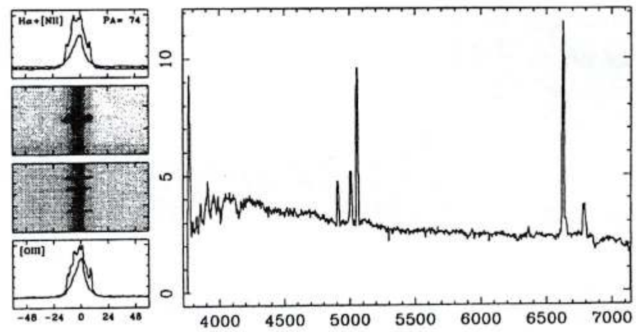

UCM0157+2413 Sy2

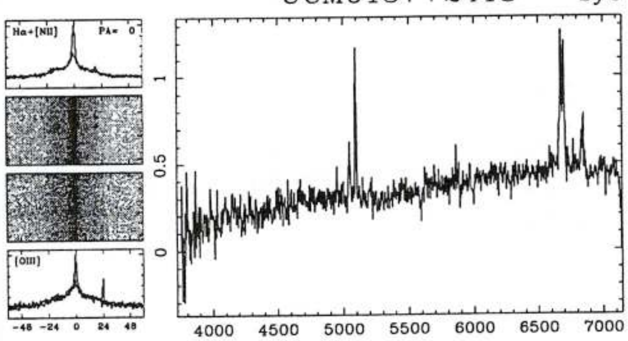

UCM0159+2326 DANS

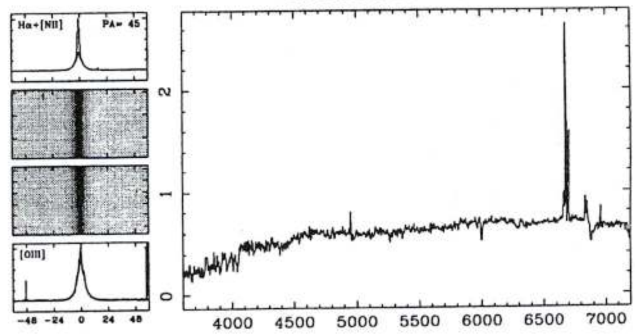

UCM1246+2727 HIIH

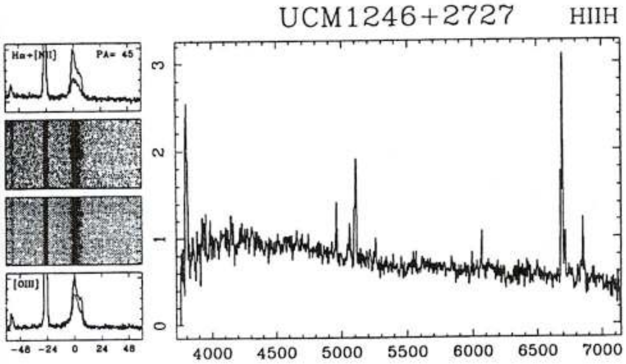

UCM1248+2912 SBN

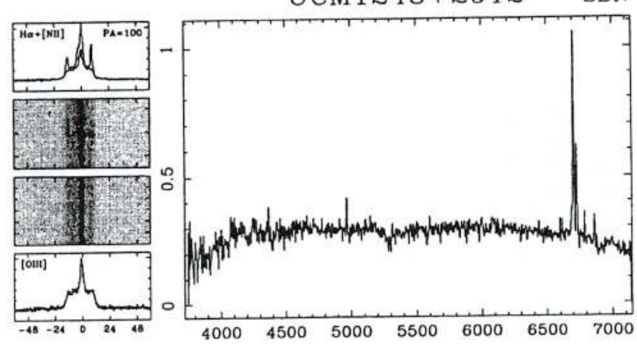

UCM1253+2756 HIIH

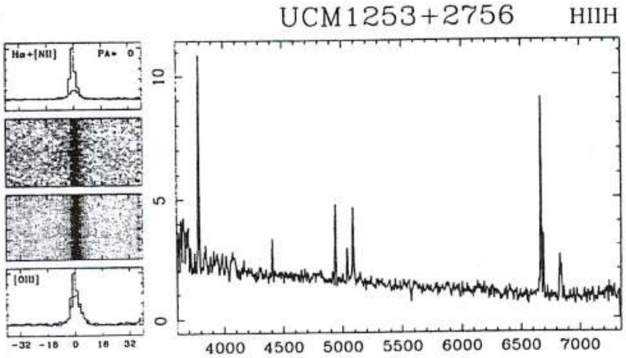

UCM1254+2741 SBN

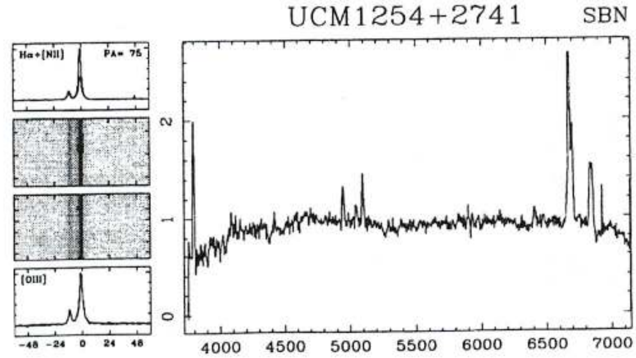

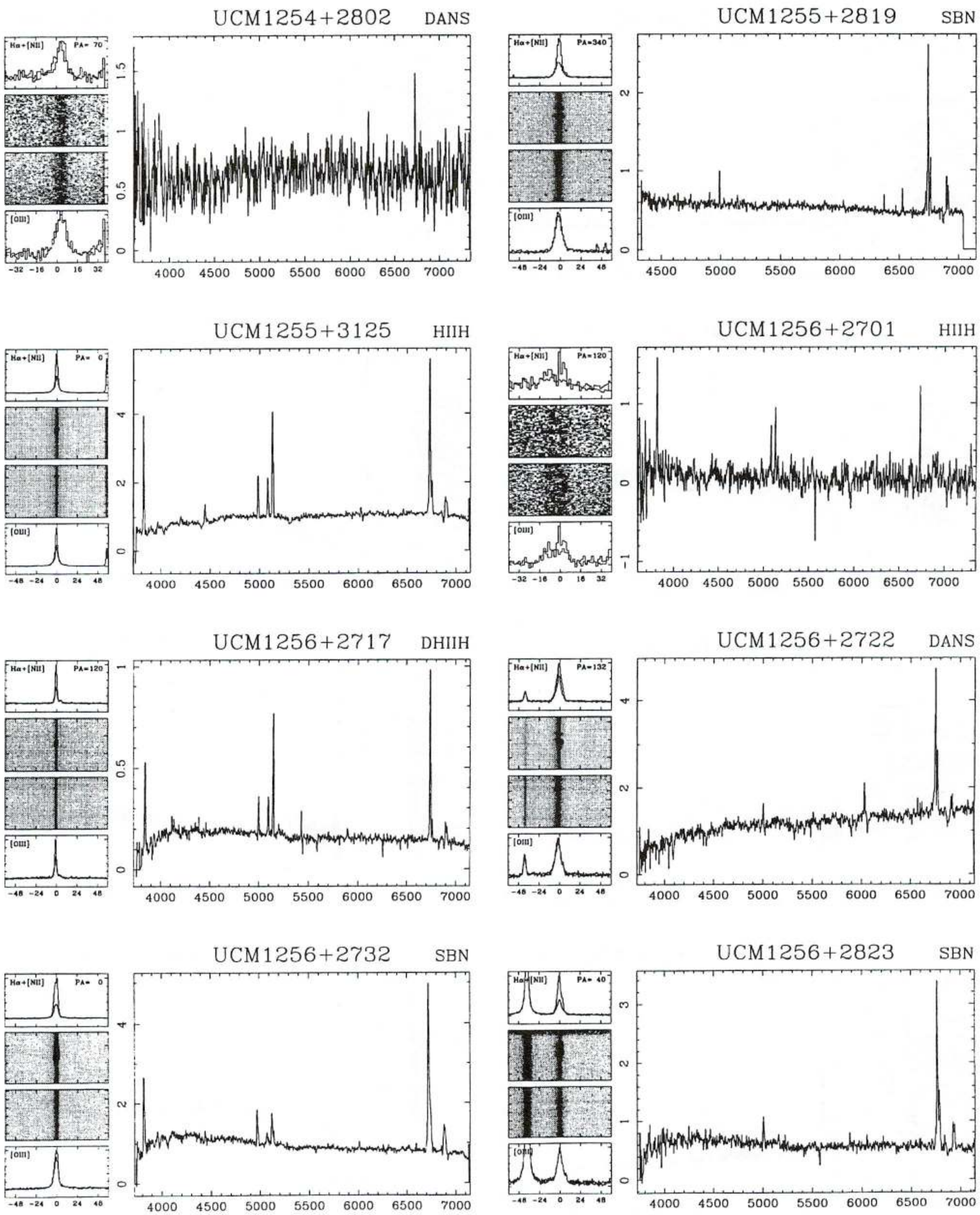
UCM1254+2802 DANS
UCM1255+2819 SBN
UCM1255+3125 HIIH
UCM1256+2701 HIIH
UCM1256+2717 DHIIH
UCM1256+2722 DANS
UCM1256+2732 SBN
UCM1256+2823 SBN
Hα+[NII]
[OIII]
PA= 70
PA=340
PA= 0
PA=120
PA=120
PA=132
PA= 0
PA= 40

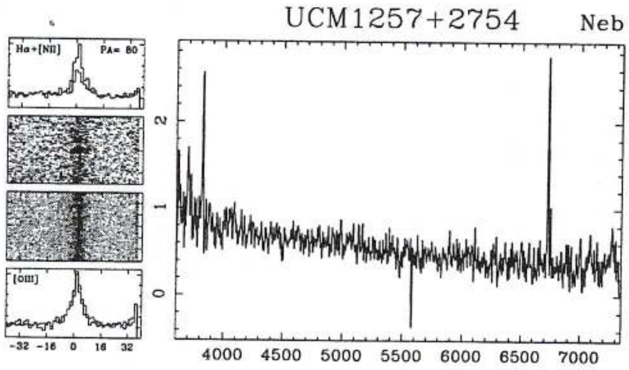
UCM1257+2754
Neb

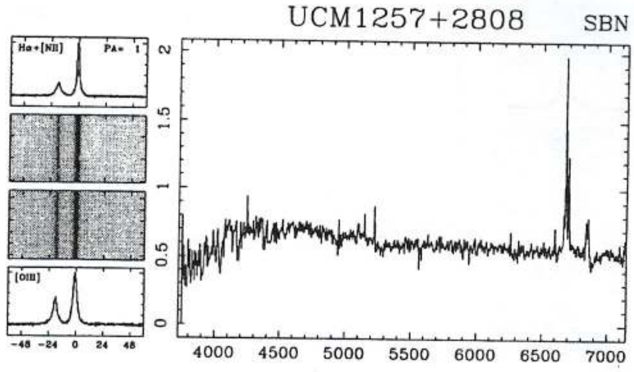
UCM1257+2808
SBN

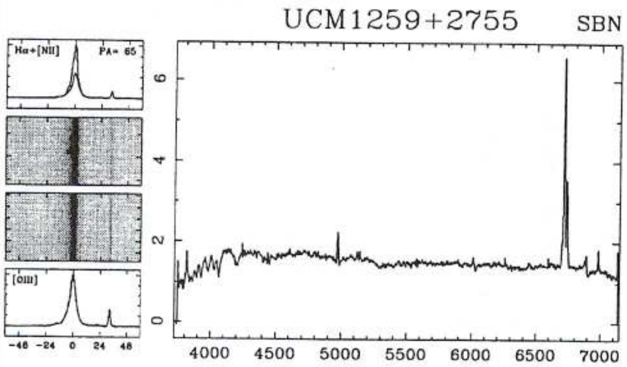
UCM1259+2755
SBN

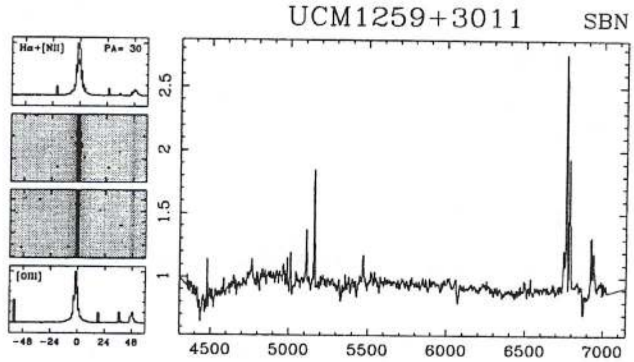
UCM1259+3011
SBN

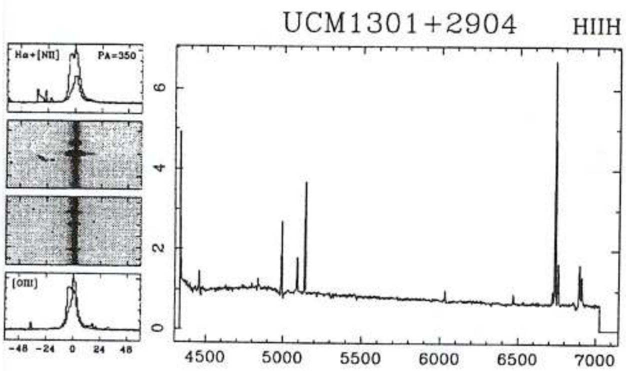
UCM1301+2904
HIIH

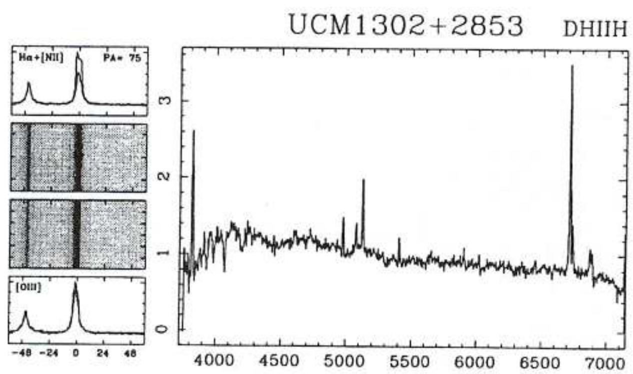
UCM1302+2853
DHIIH

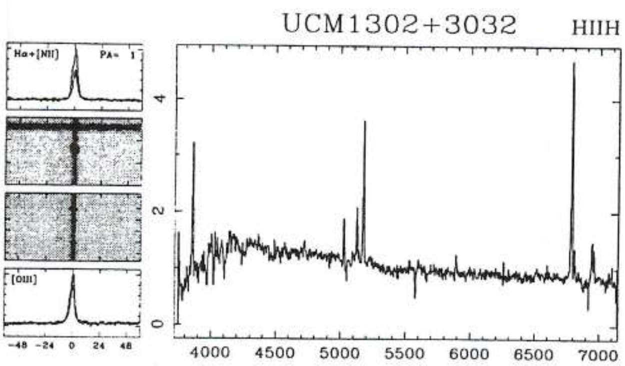
UCM1302+3032
HIIH

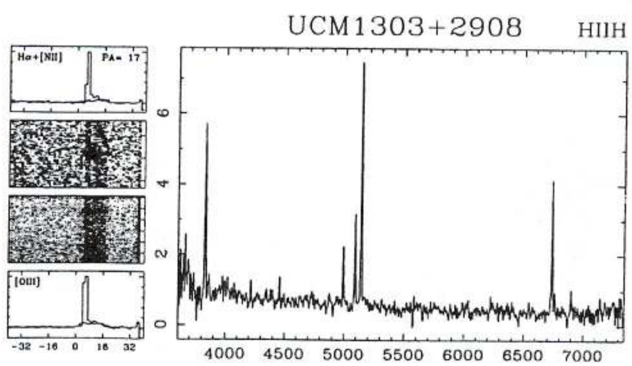
UCM1303+2908
HIIH

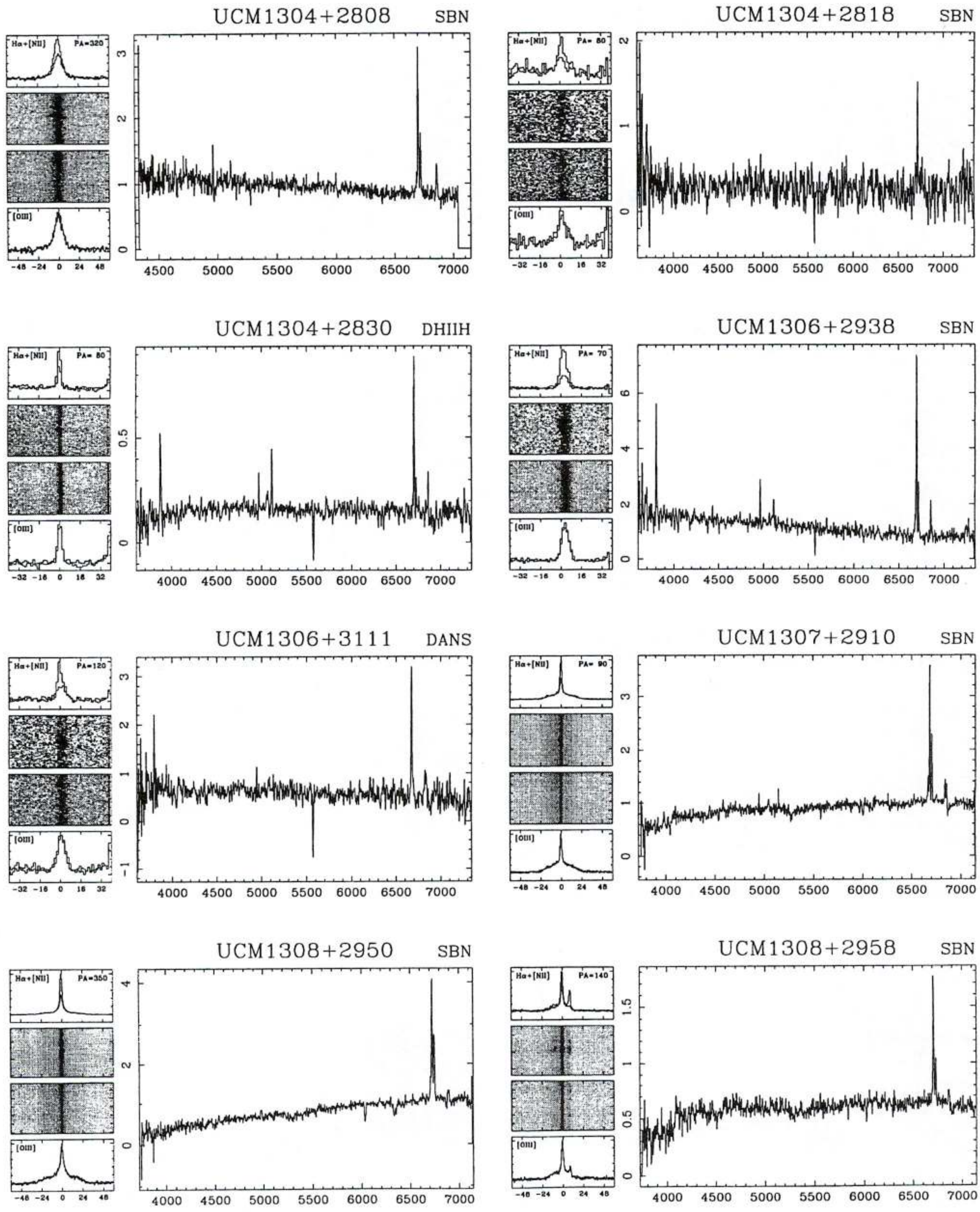
UCM1304+2808 SBN
UCM1304+2818 SBN
UCM1304+2830 DHIIH
UCM1306+2938 SBN
UCM1306+3111 DANS
UCM1307+2910 SBN
UCM1308+2950 SBN
UCM1308+2958 SBN
Hα+[NII]
[OIII]

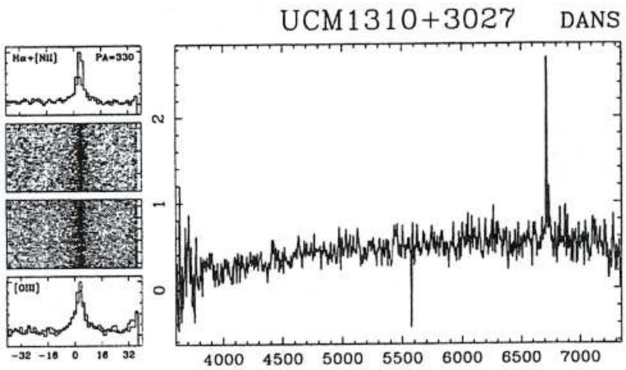
UCM1310+3027 DANS
Hα+[NII] PA=330
[OIII]

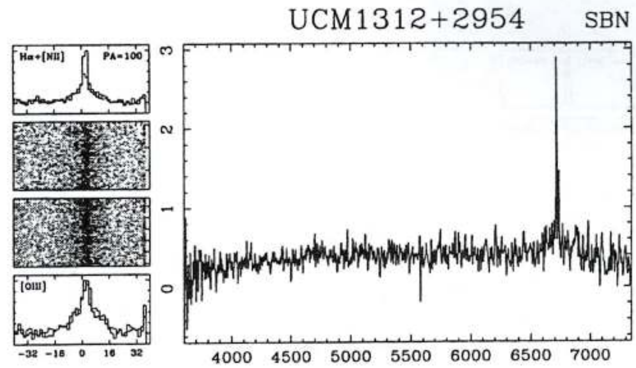
UCM1312+2954 SBN
Hα+[NII] PA=100
[OIII]

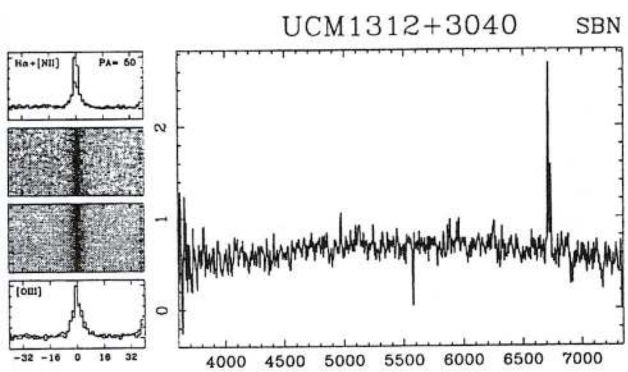
UCM1312+3040 SBN
Hα+[NII] PA= 50
[OIII]

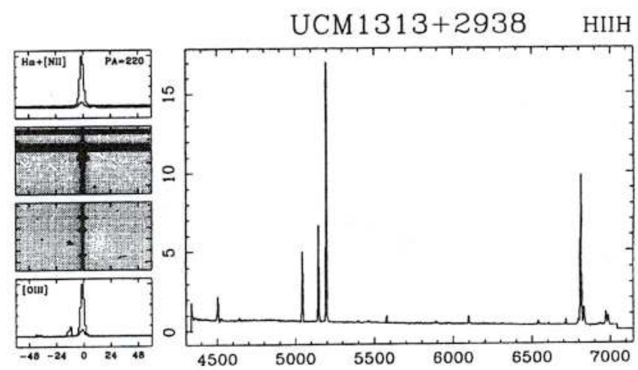
UCM1313+2938 HIIH
Hα+[NII] PA=220
[OIII]

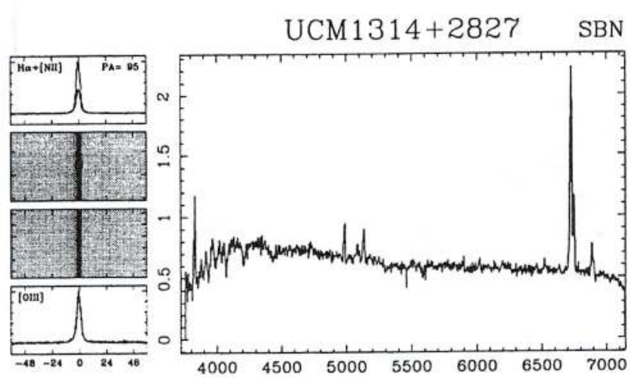
UCM1314+2827 SBN
Hα+[NII] PA= 95
[OIII]

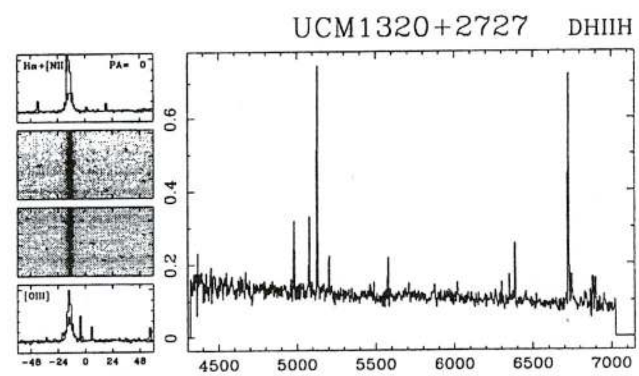
UCM1320+2727 DHIIH
Hα+[NII] PA= 0
[OIII]

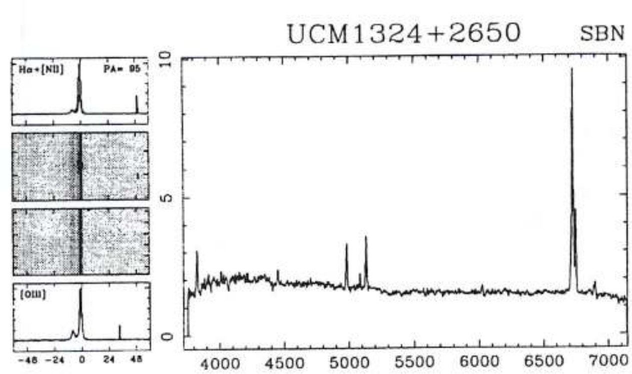
UCM1324+2650 SBN
Hα+[NII] PA= 95
[OIII]

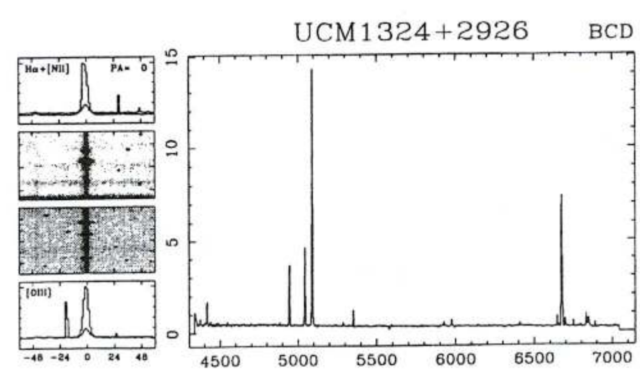
UCM1324+2926 BCD
Hα+[NII] PA= 0
[OIII]

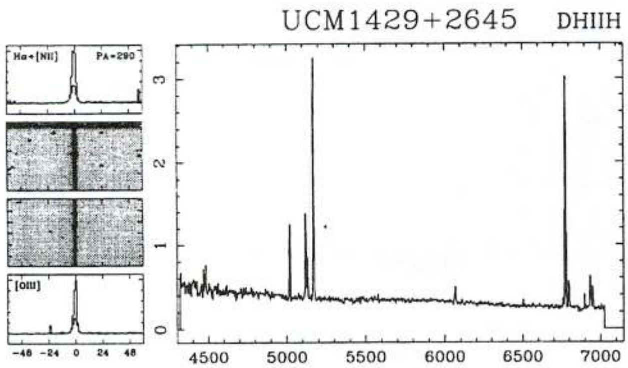
UCM1429+2645 DHIIH
Hα+[NII] PA=290
[OIII]
-48 -24 0 24 48
0 1 2 3
4500 5000 5500 6000 6500 7000

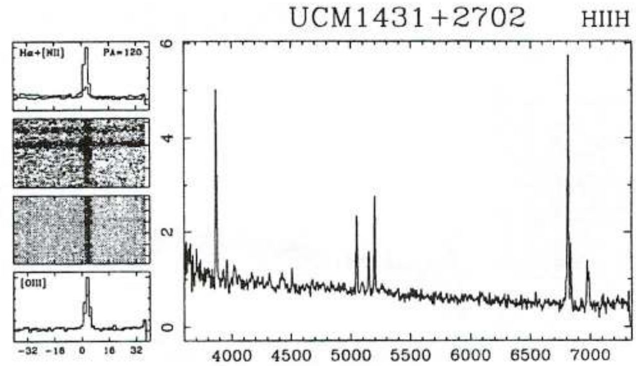
UCM1431+2702 HIIH
Hα+[NII] PA=120
[OIII]
-32 -16 0 16 32
0 2 4 6
4000 4500 5000 5500 6000 6500 7000

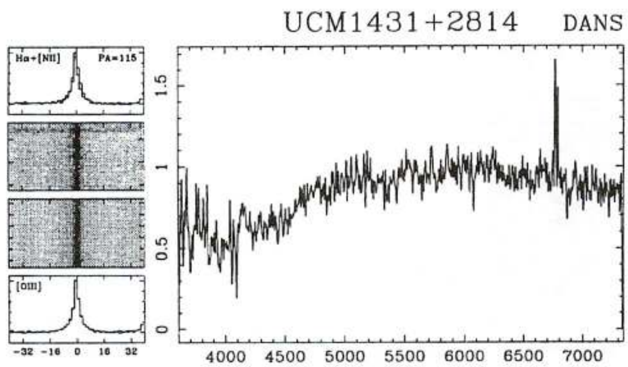
UCM1431+2814 DANS
Hα+[NII] PA=115
[OIII]
-32 -16 0 16 32
0 0.5 1 1.5
4000 4500 5000 5500 6000 6500 7000

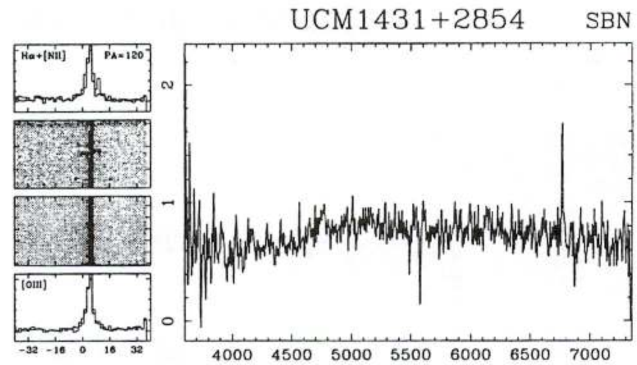
UCM1431+2854 SBN
Hα+[NII] PA=120
[OIII]
-32 -16 0 16 32
0 1 2
4000 4500 5000 5500 6000 6500 7000

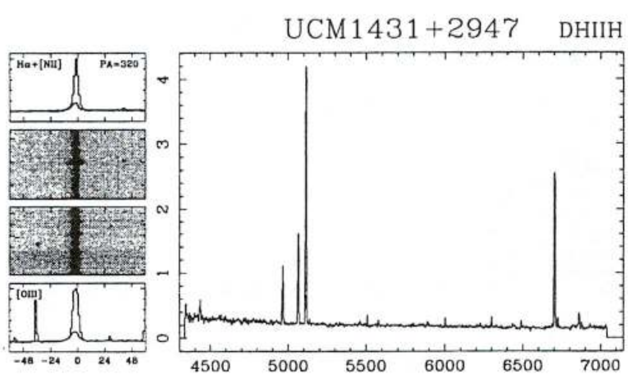
UCM1431+2947 DHIIH
Hα+[NII] PA=320
[OIII]
-48 -24 0 24 48
0 1 2 3 4
4500 5000 5500 6000 6500 7000

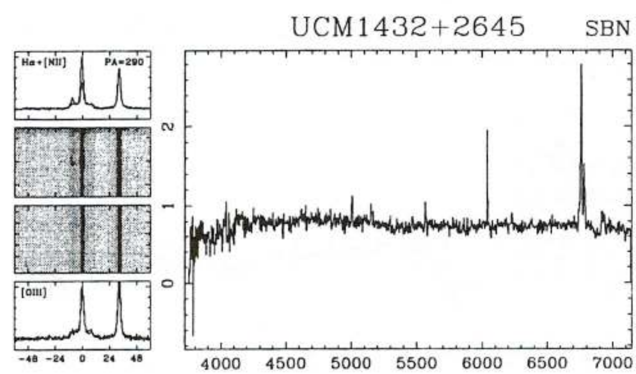
UCM1432+2645 SBN
Hα+[NII] PA=290
[OIII]
-48 -24 0 24 48
0 1 2
4000 4500 5000 5500 6000 6500 7000

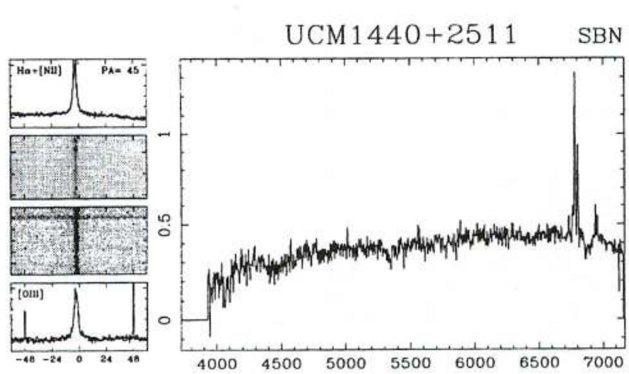
UCM1440+2511 SBN
Hα+[NII] PA= 45
[OIII]
-48 -24 0 24 48
0 0.5 1
4000 4500 5000 5500 6000 6500 7000

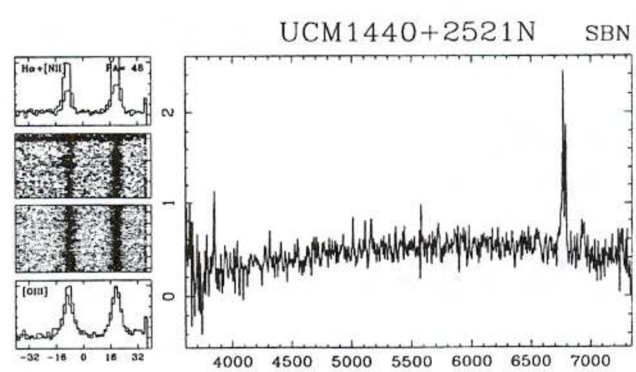
UCM1440+2521N SBN
Hα+[NII] PA= 45
[OIII]
-32 -16 0 16 32
0 1 2
4000 4500 5000 5500 6000 6500 7000

UCM1440+2521S SBN

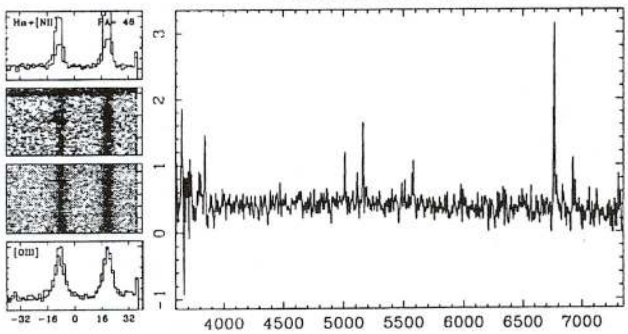

UCM1442+2845 SBN

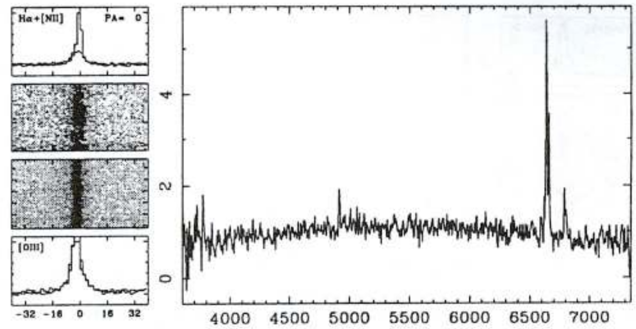

UCM1443+2548 SBN

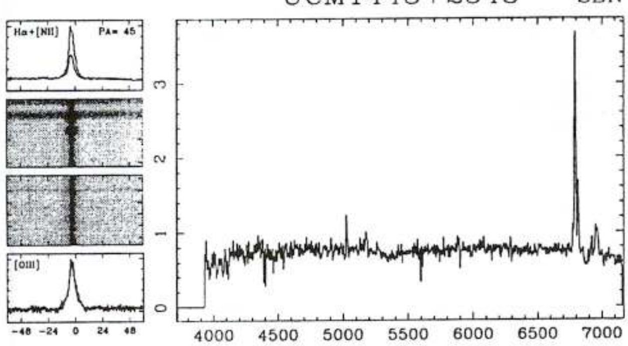

UCM1443+2714 Sy2

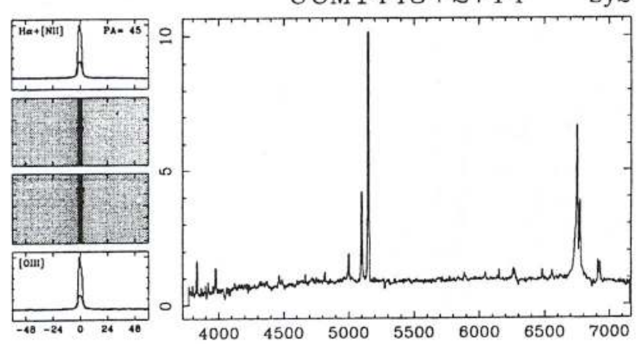

UCM1443+2844 SBN

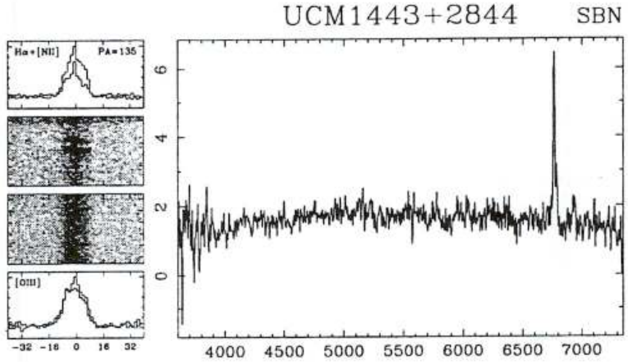

UCM1444+2923 DANS

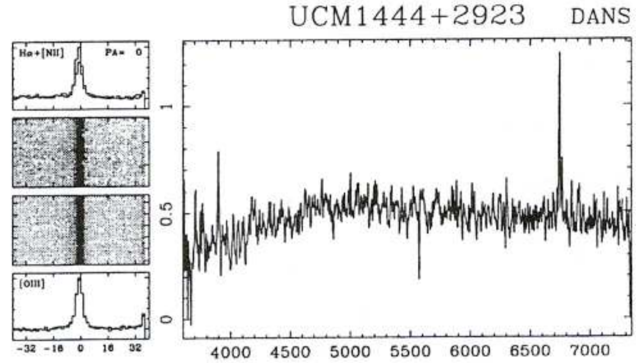

UCM1452+2754 SBN

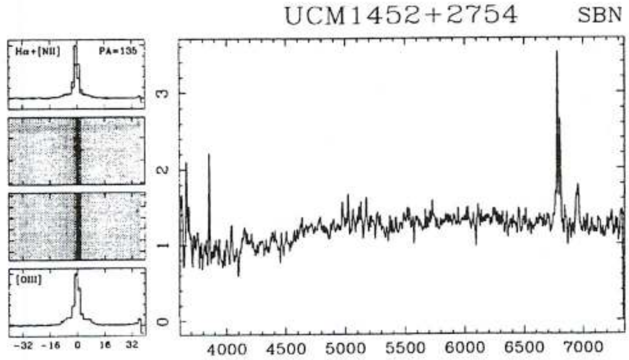

UCM1506+1922 HIIH

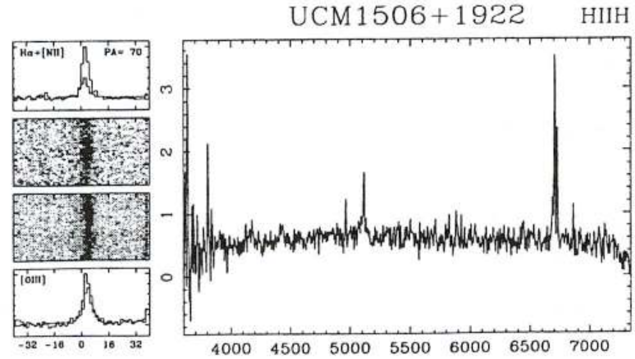

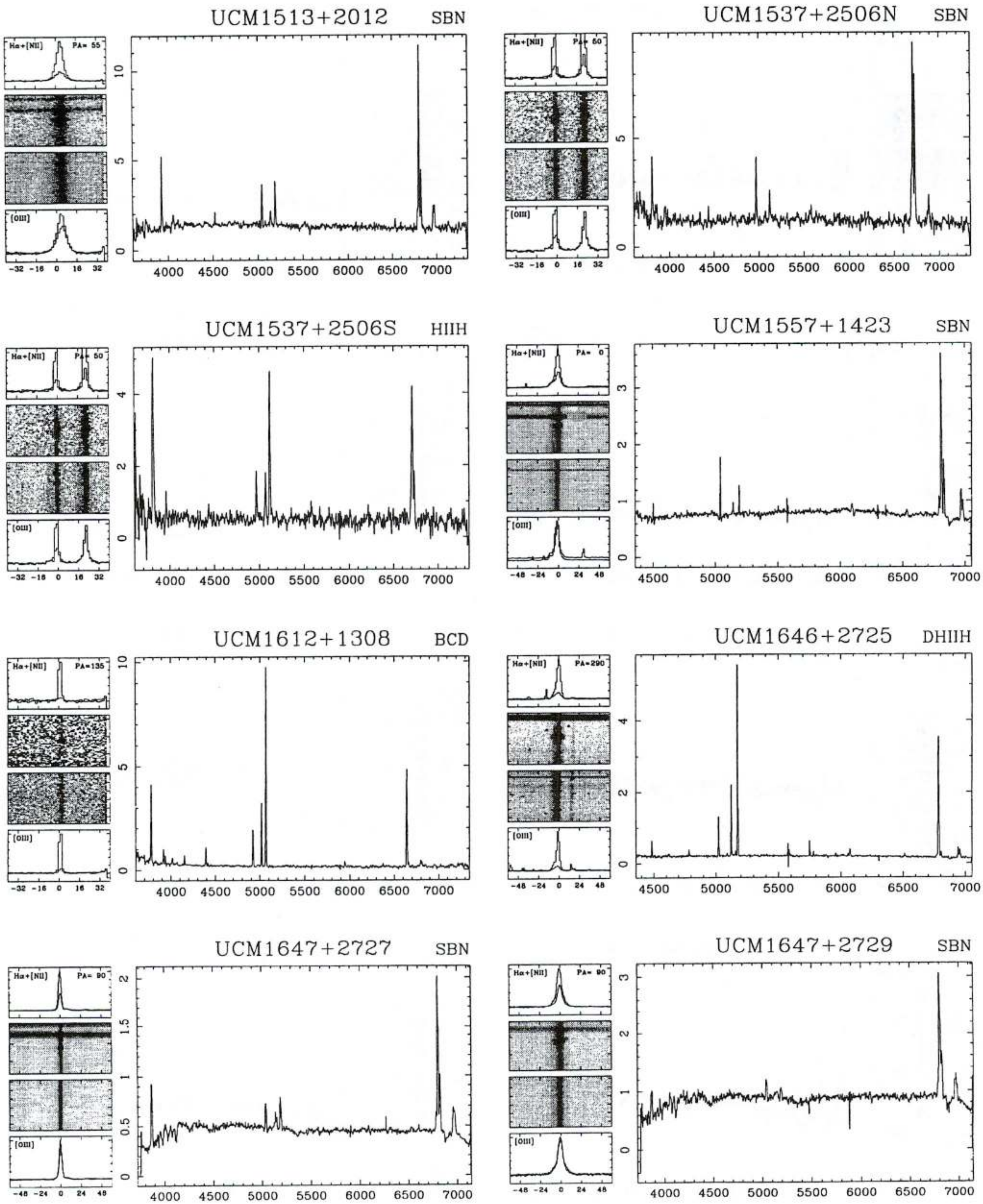
UCM1513+2012 SBN
UCM1537+2506N SBN
UCM1537+2506S HIIH
UCM1557+1423 SBN
UCM1612+1308 BCD
UCM1646+2725 DHIIH
UCM1647+2727 SBN
UCM1647+2729 SBN
Hα+[NII]
[OIII]
PA= 55
PA= 50
PA= 0
PA=135
PA=290
PA= 90

UCM1647+2950 SBN

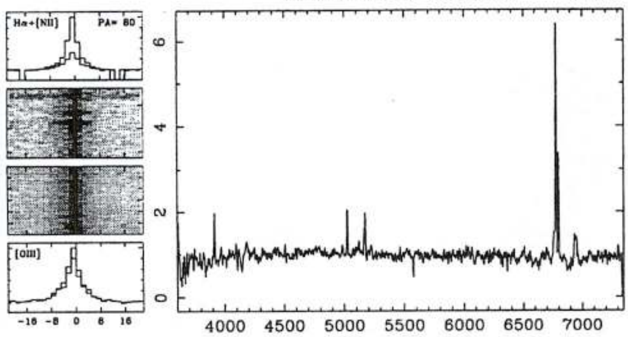

UCM1648+2855 HIIH

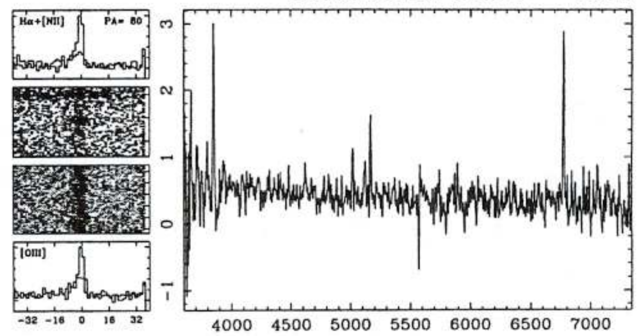

UCM1653+2644 SBN

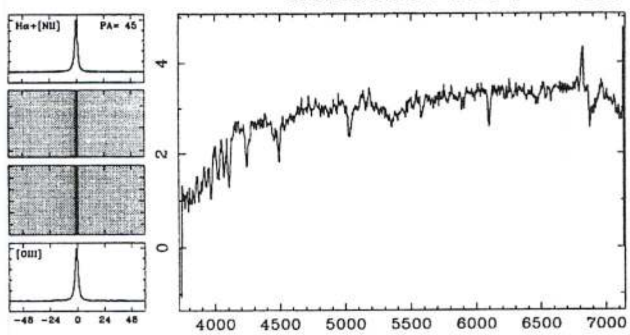

UCM1654+2812 DHIIH

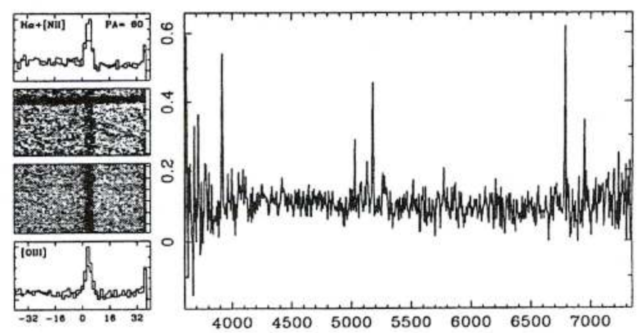

UCM1655+2755 Sy2

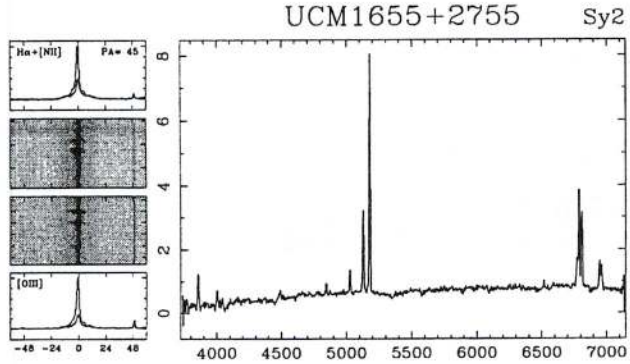

UCM1656+2744 SBN

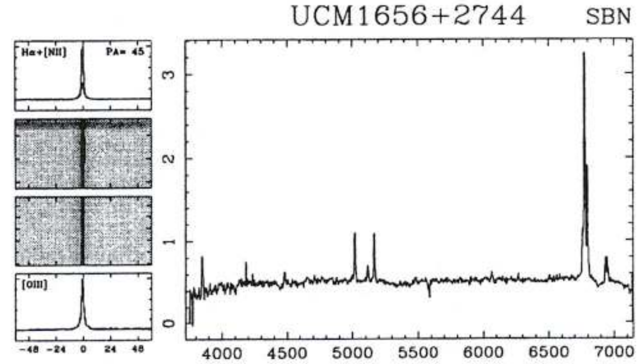

UCM1659+2928 Sy1

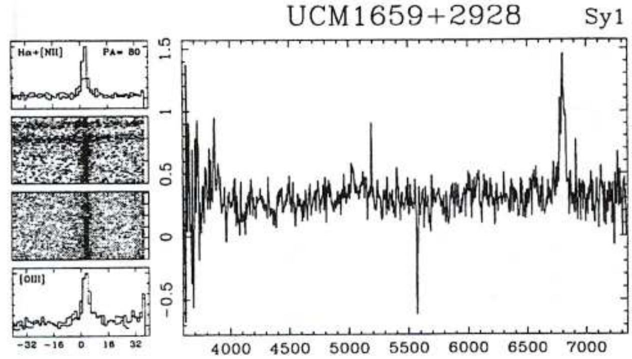

UCM1701+3131 Sy1

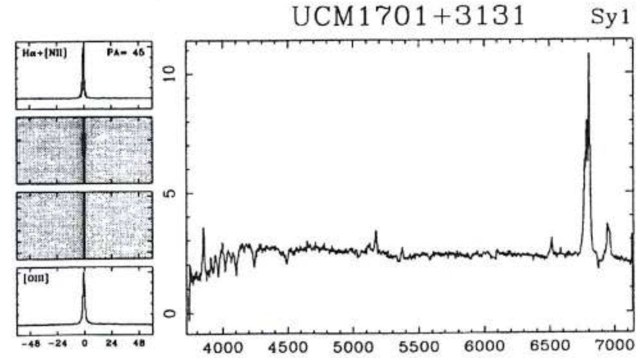

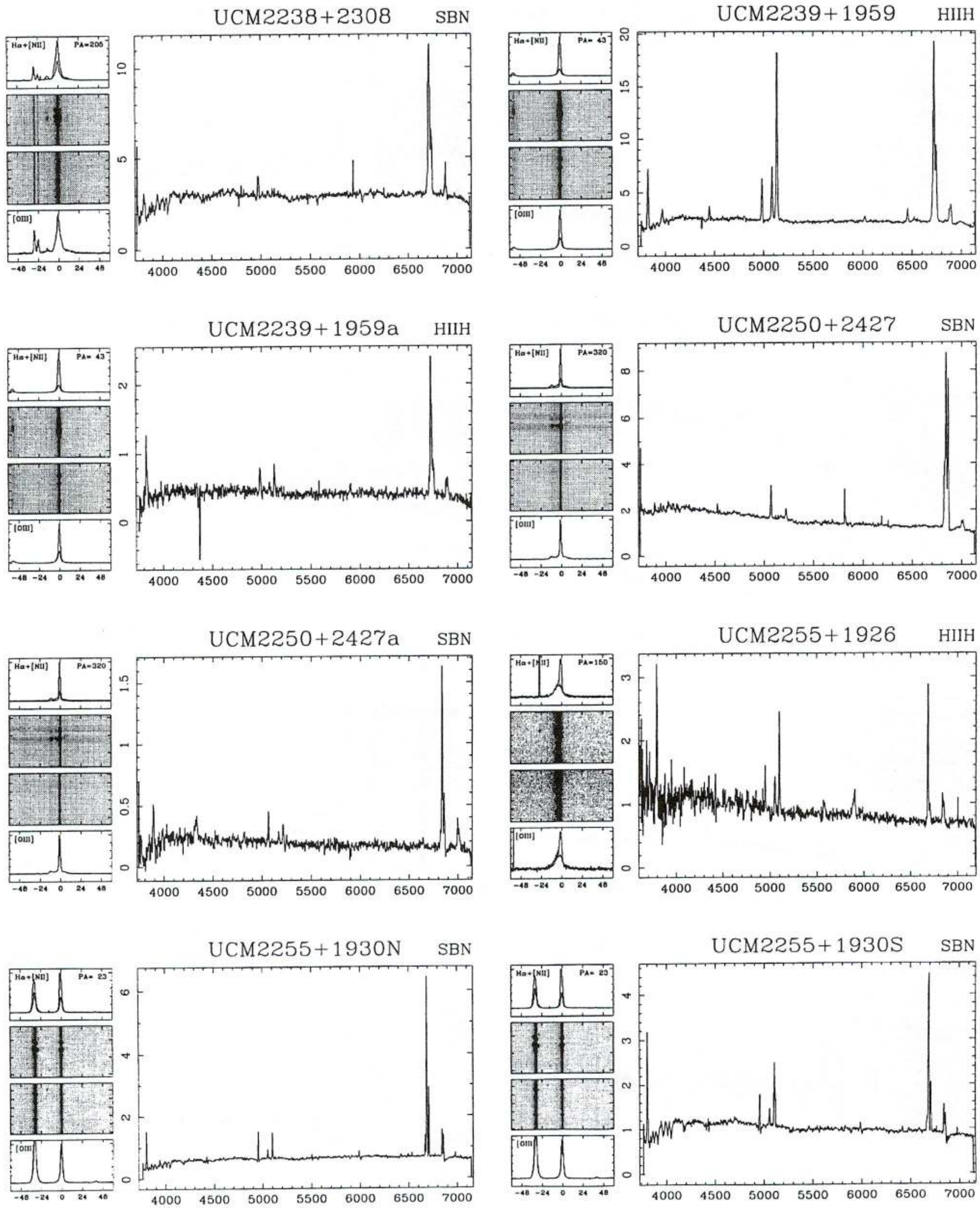
UCM2238+2308 SBN
UCM2239+1959 HIIH
UCM2239+1959a HIIH
UCM2250+2427 SBN
UCM2250+2427a SBN
UCM2255+1926 HIIH
UCM2255+1930N SBN
UCM2255+1930S SBN

UCM2256+2001 DANS

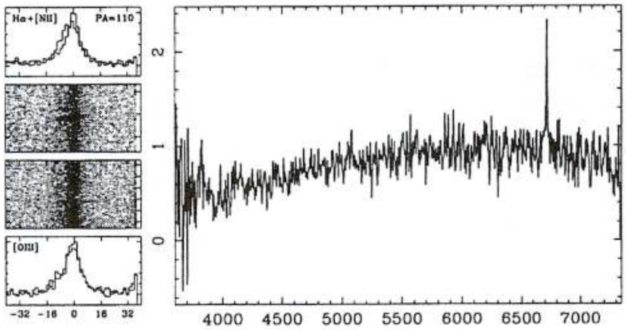

UCM2257+1606 SBN

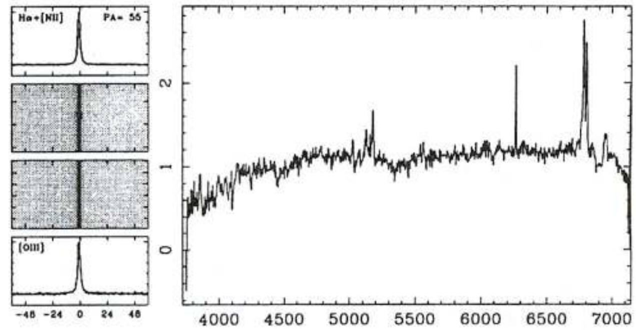

UCM2257+2438 Sy1

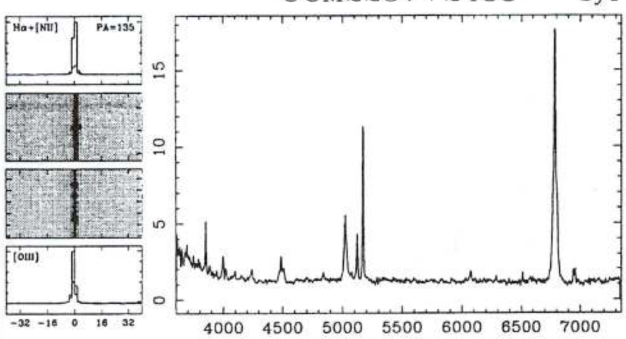

UCM2300+2015 SBN

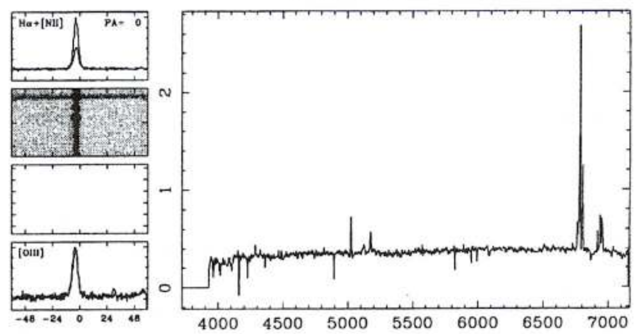

UCM2302+2053E HIIH

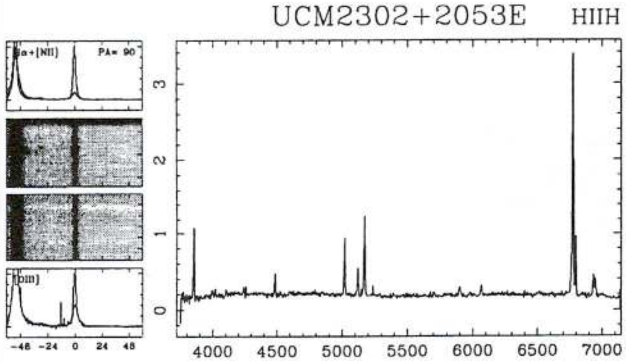

UCM2302+2053W SBN

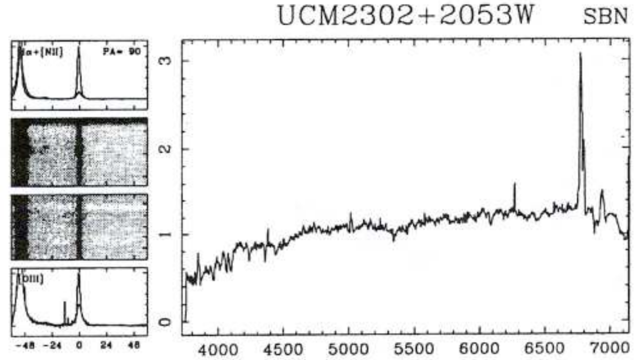

UCM2303+1702 Sy2

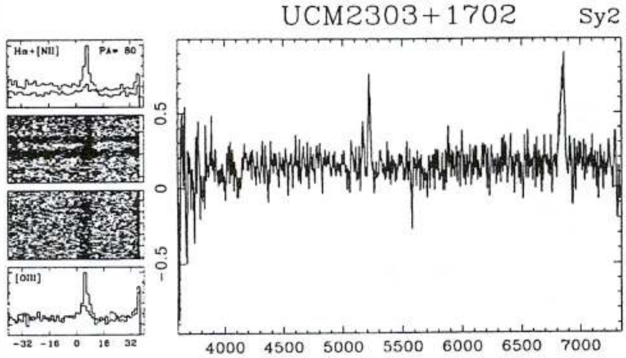

UCM2303+1856 SBN

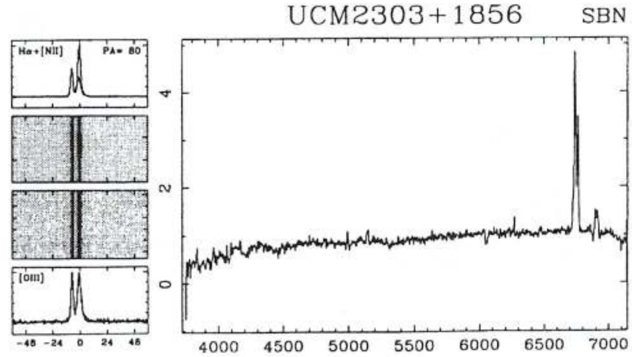

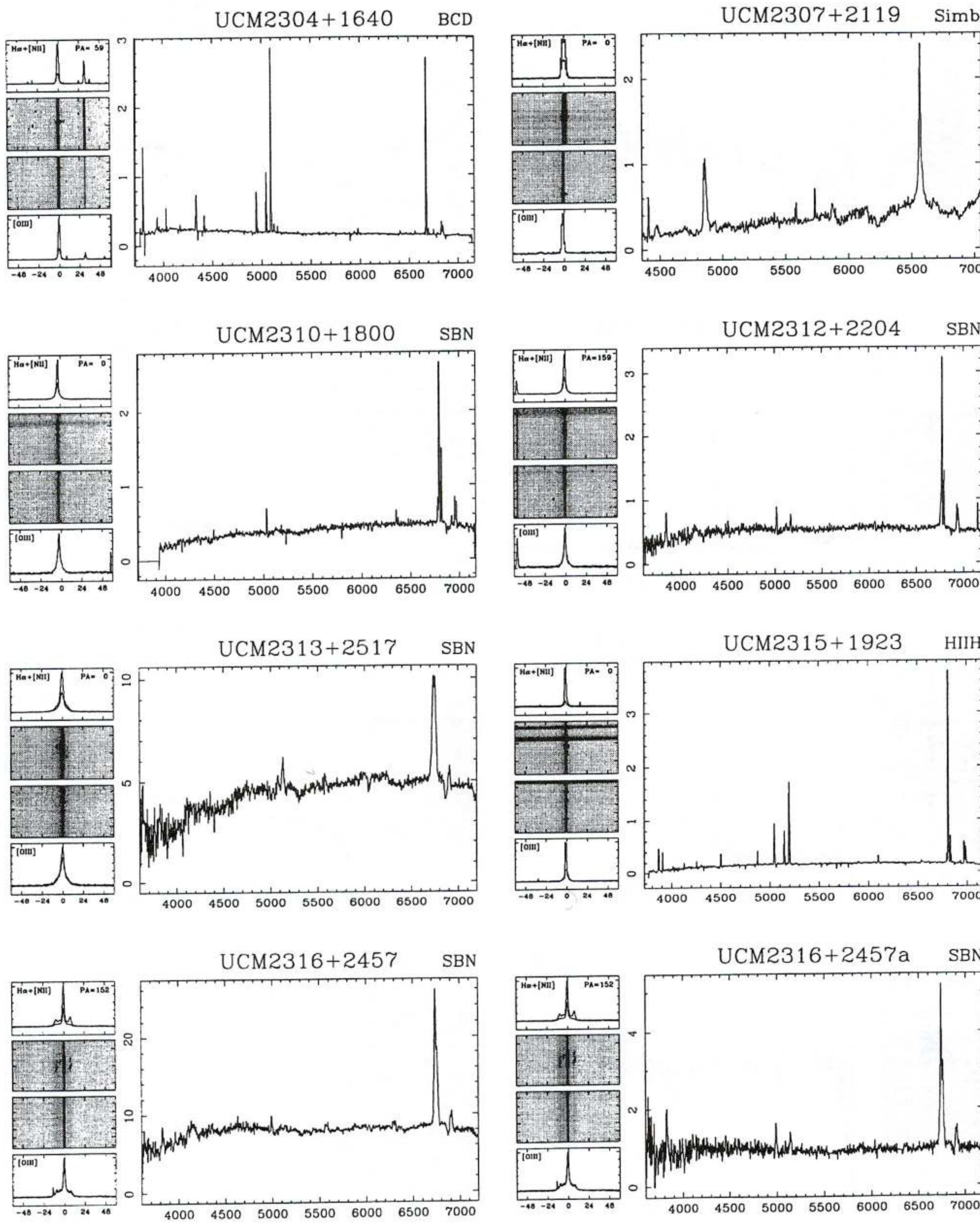
UCM2304+1640 BCD
UCM2307+2119 Simb
UCM2310+1800 SBN
UCM2312+2204 SBN
UCM2313+2517 SBN
UCM2315+1923 HIIH
UCM2316+2457 SBN
UCM2316+2457a SBN
Hα+[NII]
[OIII]
PA= 59
PA= 0
PA=159
PA=152
4000 4500 5000 5500 6000 6500 7000

UCM2316+2457b SBN

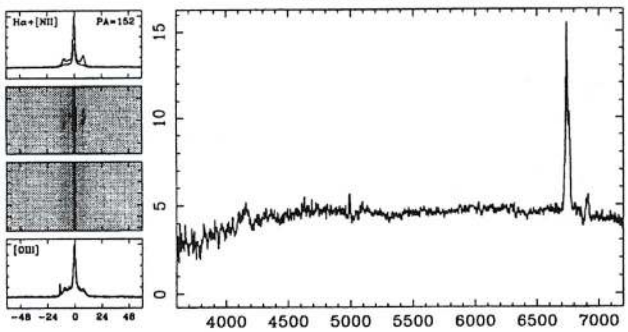

UCM2316+2457c SBN

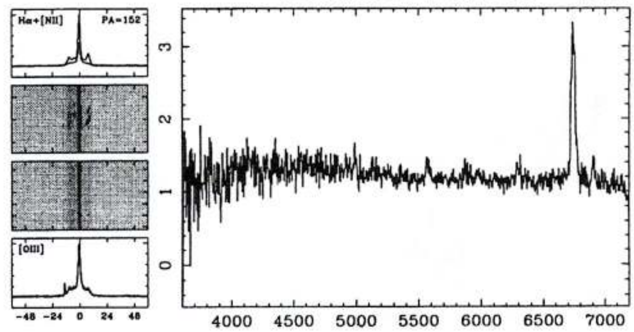

UCM2316+2459 SBN

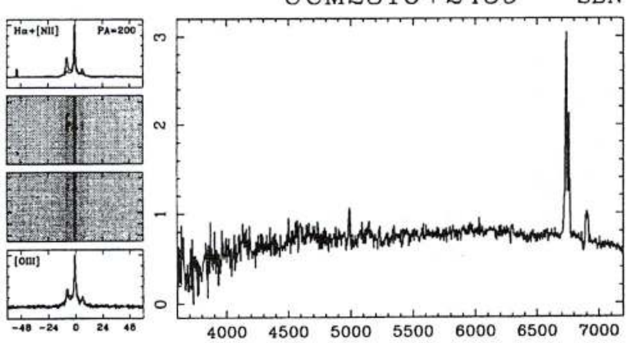

UCM2316+2459b SBN

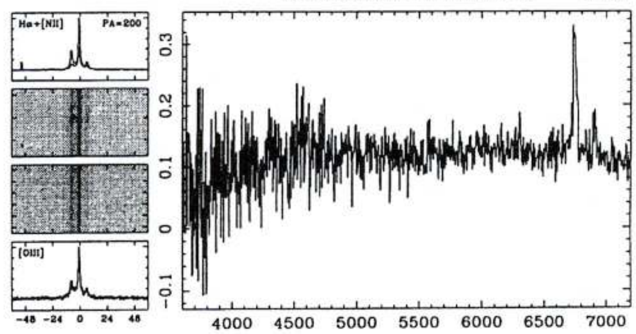

UCM2316+2459c SBN

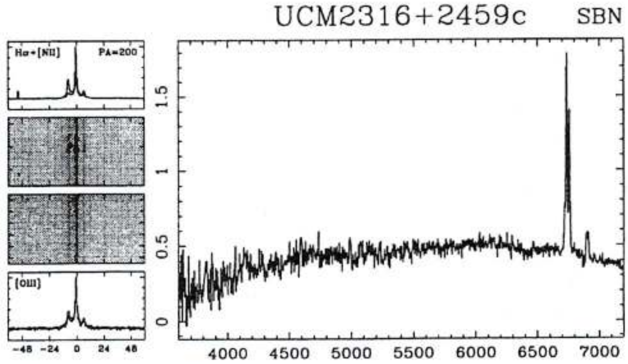

UCM2316+2459d SBN

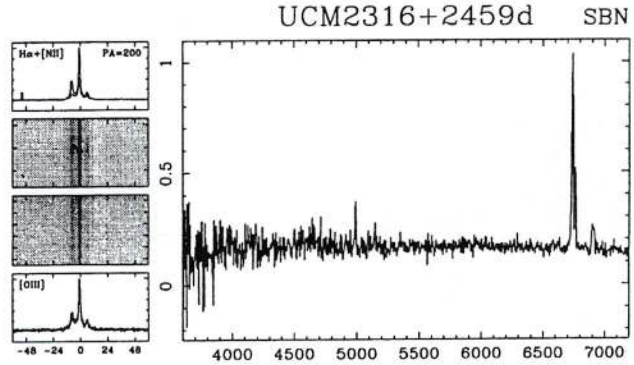

UCM2317+2356 SBN

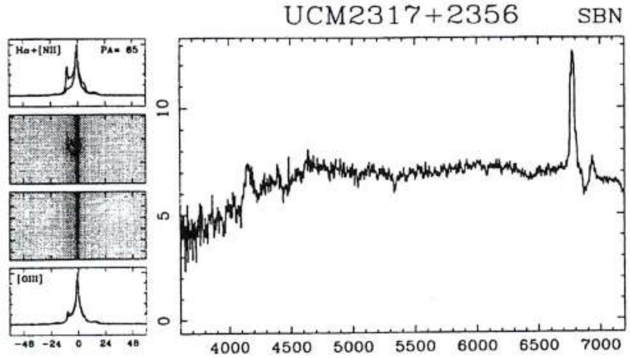

UCM2317+2356a LINER

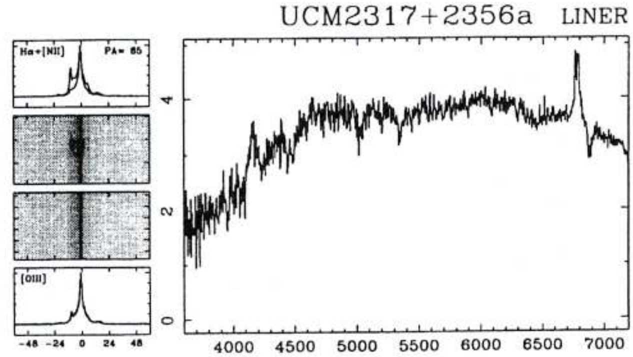

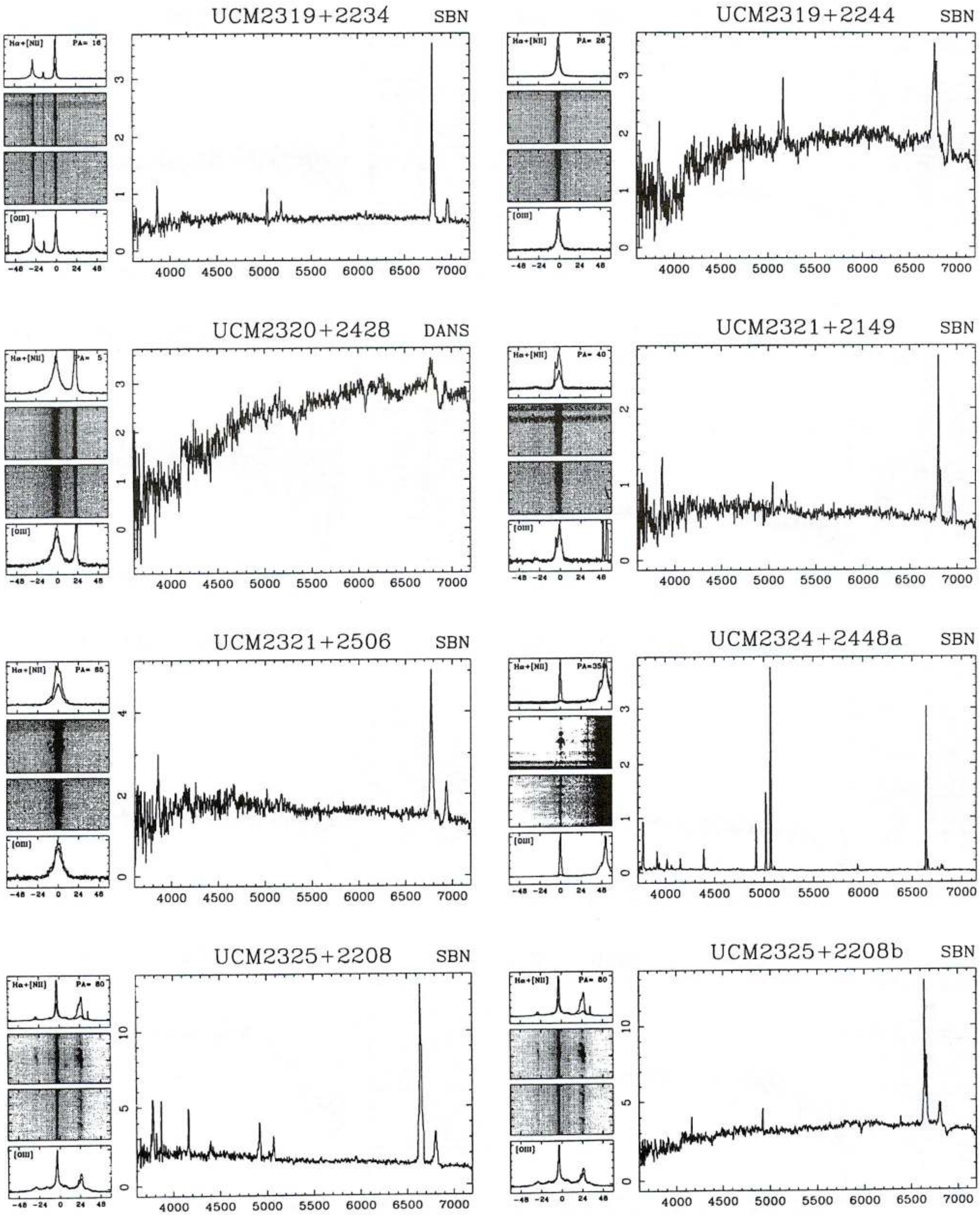
UCM2319+2234 SBN
UCM2319+2244 SBN
UCM2320+2428 DANS
UCM2321+2149 SBN
UCM2321+2506 SBN
UCM2324+2448a SBN
UCM2325+2208 SBN
UCM2325+2208b SBN

UCM2325+2208c SBN

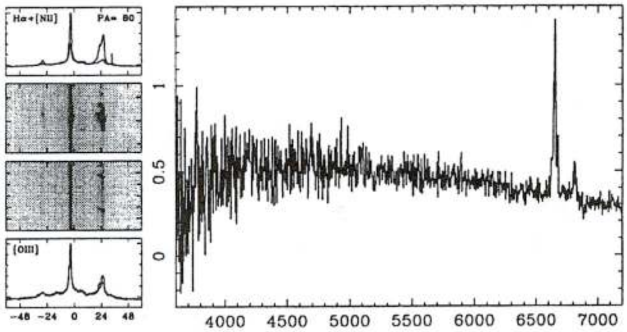

UCM2325+2318 HIIH

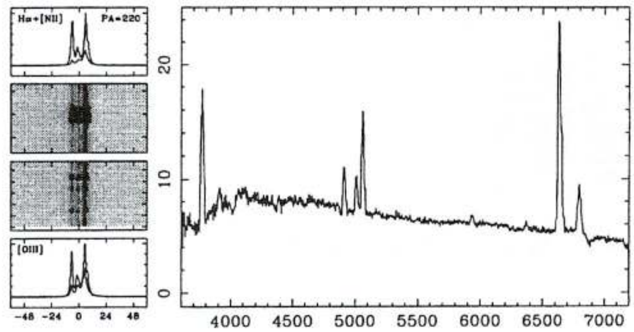

UCM2325+2318b HIIH

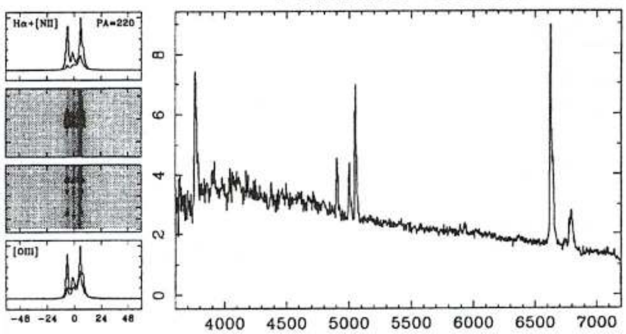

UCM2325+2318c HIIH

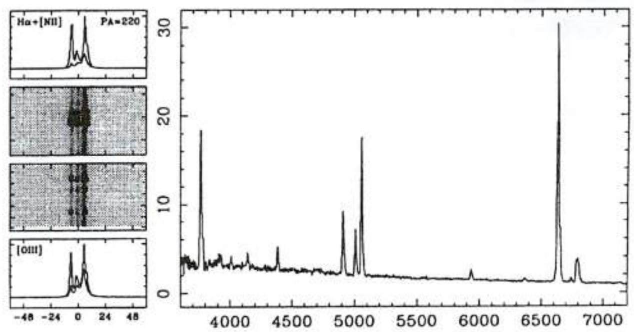

UCM2326+2435 DHIIH

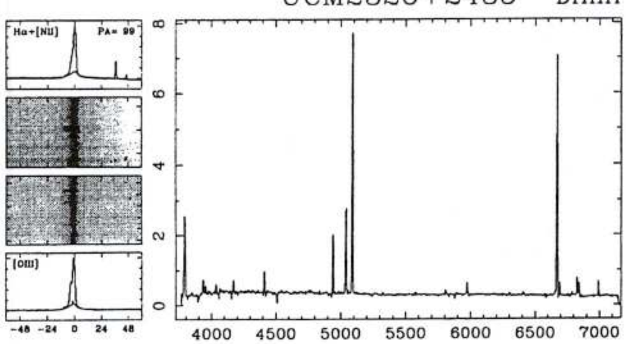

UCM2327+2515S HIIH

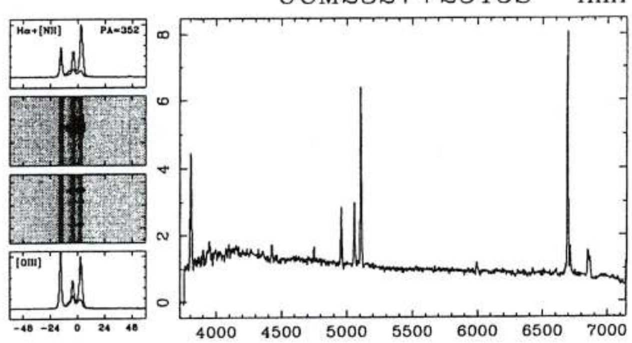

UCM2327+2515N HIIH

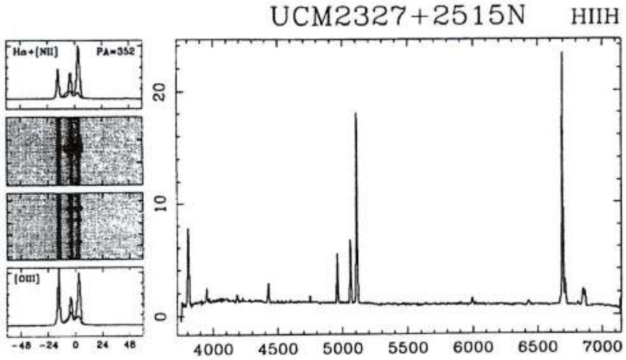

UCM2329+2427 DANS

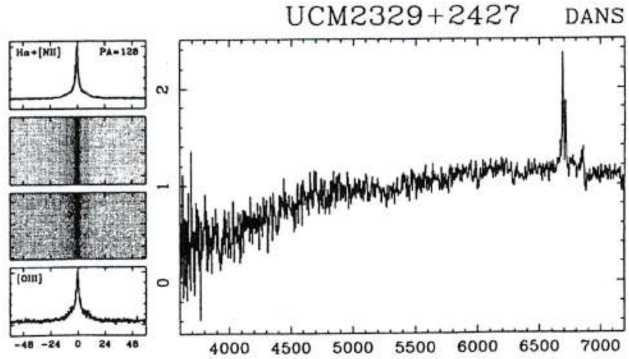

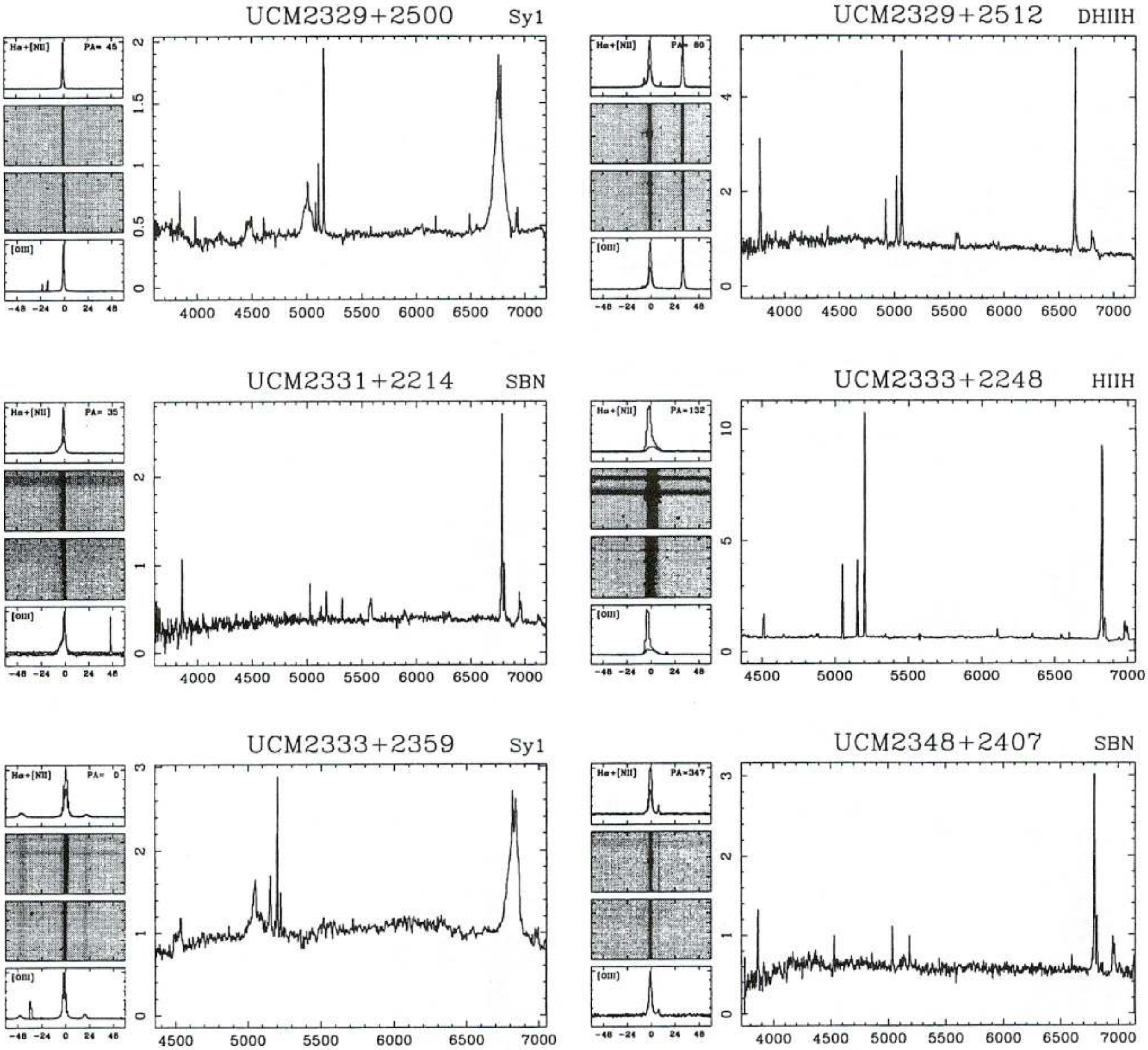
UCM2329+2500 Sy1
Hα+[NII] PA= 45
[OIII]
UCM2329+2512 DHIIH
Hα+[NII] PA= 80
[OIII]
UCM2331+2214 SBN
Hα+[NII] PA= 35
[OIII]
UCM2333+2248 HIIH
Hα+[NII] PA=132
[OIII]
UCM2333+2359 Sy1
Hα+[NII] PA= 0
[OIII]
UCM2348+2407 SBN
Hα+[NII] PA=347
[OIII]